Water Vapor Effect on the HNO$_3$ Yield in the HO$_2$ + NO Reaction: Experimental and Theoretical Evidence

Nadezhda Butkovskaya,*,† **Marie-Thérèse Rayez,**‡ **Jean-Claude Rayez,**‡ **Alexandre Kukui,**§ **and Georges Le Bras**†
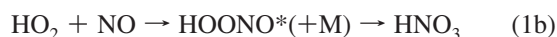
CNRS, Institut de Combustion, Aérothermique, Réactivité et Environnement (ICARE), 1C Av. de la Recherche Scientifique, 45071 Orléans Cedex 2, France, Université Bordeaux1/CNRS- Institut des Sciences Moléculaires (ISM-UMR5255), 351 Cours de la Libération, 33405 Talence Cedex, France, and CNRS Service Laboratoire Atmosphères, Milieux, Observations Spatiales (LATMOS), 91371 Verrières-le-Buisson, France

The influence of water vapor on the production of nitric acid in the gas-phase HO$_2$ + NO reaction was determined at 298 K and 200 Torr using a high-pressure turbulent flow reactor coupled with a chemical ionization mass spectrometer. The yield of HNO$_3$ was found to increase linearly with the increase of water concentration reaching an enhancement factor of about 8 at [H$_2$O] = 4 × 10^{17} molecules cm^{-3} (~50% relative humidity). A rate constant value $k_{1bw} = 6 \times 10^{-13}$ cm^3 molecule^{-1} s^{-1} was derived for the reaction involving the HO$_2$·H$_2$O complex: HO$_2$·H$_2$O + NO → HNO$_3$ (1bw), assuming that the water enhancement is due to this reaction. k_{1bw} is approximately 40 times higher than the rate constant of the reaction HO$_2$ + NO → HNO$_3$ (1b), at the same temperature and pressure. The experimental findings are corroborated by density functional theory (DFT) calculations performed on the H$_2$O/HO$_2$/NO system. The significance of this result for atmospheric chemistry and chemical amplifier instruments is briefly discussed. An appendix containing a detailed consideration of the possible contribution from the surface reactions in our previous studies of the title reaction and in the present one is included.

I. Introduction

Water vapor has been found to significantly enhance the rate constant of the HO$_2$ self-reaction.[1−5] The enhancement is explained by a catalytic effect of water vapor due to the formation of the HO$_2$·H$_2$O complex. A similar mechanism may occur in other HO$_2$ radical reactions, in particular, the HO$_2$ + NO reaction (1a and 1b). Recently, we have determined the branching ratio for this reaction, $\beta = k_{1b}/k_{1a}$, over a wide range of pressures and temperatures relevant for the troposphere,[6] with some indication of its dependence on water vapor concentration.[7] It is supposed that the reaction proceeds through the formation of the HOONO intermediate complex that rapidly decomposes into OH and NO$_2$ with a small fraction forming HNO$_3$ through isomerization[8−10]

$$\text{HO}_2 + \text{NO} \rightarrow \text{HOONO}^* \rightarrow \text{OH} + \text{NO}_2 \qquad (1a)$$

$$\text{HO}_2 + \text{NO} \rightarrow \text{HOONO}^*(+\text{M}) \rightarrow \text{HNO}_3 \qquad (1b)$$

The branching ratio was found to be 0.17% at $P = 200$ Torr and $T = 298$ K.[6] Recent model calculations[11] showed that the obtained yield of HNO$_3$, although very low, has a significant impact on the atmospheric concentrations of HO$_x$, NO$_x$, HNO$_3$,

and ozone species, because the termination reaction (1b) plays an important role in the key atmospheric cycles of OH initiated oxidation of volatile organic compounds and CO. Accordingly, for atmospheric modeling, the humidity effect on reaction 1b must be carefully examined. Another important aspect is that reaction 1a is a propagating step in the chain mechanism used to convert low concentrations of HO$_2$ into measurable NO$_2$ concentrations for the detection of atmospheric RO$_2$ radicals by the chemical amplifier instruments (e.g., ref 12). Detection sensitivity of chemical amplifiers was found to decrease with increasing relative humidity, and chain termination reaction 1b has been suggested as a possible cause of the decrease of the chain length.[13]

In the present work, the effect of water on the nitric acid formation in the HO$_2$ + NO reaction has been investigated at room temperature and pressure of 200 Torr using a turbulent flow reactor (TFR) coupled with a chemical ionization mass spectrometer (CIMS). The experimental study was complicated by a strong impact of water on the processes in the ion−molecule reactor (IMR). It was found that introduction of large concentrations of H$_2$O into the TFR leads to overall decrease of concentrations of primary negative ions in the IMR and, hence, to changes in the detection process. An accompanying study of water dependence for some clustering and other background reactions was needed to discriminate between the water effect on the ion source processes and that on HNO$_3$ formation in reaction 1. In particular, this was achieved using heavy water, D$_2$O.

As the nitric acid yield from (1b) is only a small fraction of the total reaction, chemical interferences including surface reactions must be carefully considered both with and without water vapor. In our first publication on this reaction we have already discussed a possible influence of the reactor walls on

---

* Corresponding author, bout@cnrs-orleans.fr. Permanent address: Institute of Chemical Physics of the Russian Academy of Sciences, 117334 Moscow, Russian Federation.
† CNRS, Institut de Combustion, Aérothermique, Réactivité et Environnement (ICARE).
‡ Université Bordeaux1/CNRS- Institut des Sciences Moléculaires (ISM-UMR5255).
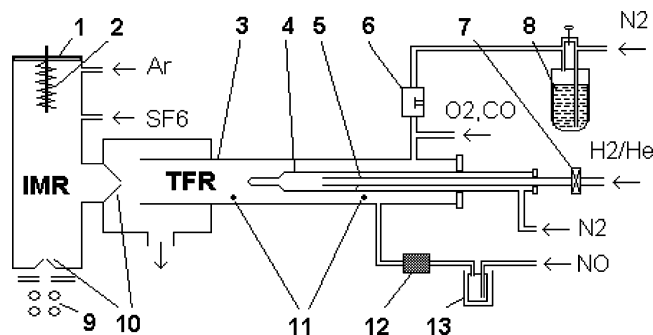§ CNRS, Laboratoire Atmosphères, Milieux, Observations Spatiales (LATMOS).

Figure 1. Experimental setup: 1, ion molecule reactor (IMR); 2, ion source; 3, turbulent flow reactor (TFR); 4, moveable injector; 5, discharge tube; 6, hygrometer; 7, surfatron (microwave discharge); 8, water bubbler; 9, quadrupole mass analyzer; 10, sampling cones; 11, thermocouples; 12, $Fe^{II}(SO_4)$ filter; 13, liquid N_2/ethanol cold bath.

the nitric acid observations.[7] Since new questions arose after the study of the pressure dependence at different temperatures,[6] an Appendix with more detailed consideration of the possible contribution from the surface reaction supplements the present publication.

In parallel with the experimental study, a theoretical investigation has been undertaken. The aim was to search for all the mechanisms that lead to the formation of HNO_3 from the HO_2 + NO reaction and to analyze the role of water vapor in the formation of HNO_3. Our general theoretical approach was the determination of the singlet potential energy surface (PES) involved in the reaction. Several publications[8-10,14] exist on theoretical study of reaction 1a or on the fate of the activated HOONO complex[15,16] that have been already discussed in the context of the experimental results on the HNO_3 yield.[6,7] All of them are not fully conclusive, especially regarding the HOONO/ HNO_3 isomerization pathways. Zhang and Donahue,[10] in their master equation simulation of the HO_2 + NO/OH + NO_2 system taking into account all the existing experimental constraints, have found a noncontradictory set of PES parameters giving HNO_3 yield in agreement with the experimental HNO_3 production at least for 298 K. However, the postulated parameters are not completely consistent with the available computational results. More recently, Chen et al.[17,18] have reported quasi-classical trajectory calculations on a global analytic potential energy surface for the reaction HO_2 + NO fitted on a large number of B3LYP/6-311G(d,p) calculated electronic energies. All the trajectories show the formation of HOONO complexes which mainly decompose to OH + NO_2 and, for a very small part, isomerize to $HONO_2$. In the present work, we have revisited the pathways leading to HO + NO_2 and HNO_3 products, using the DFT-UB3LYP approach at the unrestricted level described in section III. Our objective was, in a first step, to find a semiquantitative model describing all the channels of the HO_2 + NO reaction and, in a second step, to search how this model is perturbed by the addition of one H_2O molecule to the HO_2/NO system.

II. Experimental Study

II.1. Experimental Methods. *Chemical Reactor.* The experimental setup consisting of a high-pressure turbulent flow reactor coupled to a chemical ionization mass spectrometer has been already used in our earlier studies of the HO_2 + NO reaction.[6,7] A scheme of the apparatus is presented in Figure 1. The flow in the TFR was created by N_2 carrier gas evaporating from a liquid nitrogen tank. The working pressure was 200 Torr at flow rates of about 60 SLPM corresponding to a Reynolds

number of about 5500. The temperature in the TFR, $T = 298 \pm 1$ K, corresponded to the ambient room temperature. The HO_2 radicals were produced in the TFR by the combination reaction of H atoms with O_2, with H atoms generated by a microwave discharge in H_2/He gas mixtures flowing through a quartz tube concentrically connected to the movable injector. Flows of N_2 in the injector and of He in the discharge tube were optimized for maximum H atom production. He (AlphaGaz 2) was purified by passing through molecular sieves cooled by liquid N_2. Tank grade H_2 (AlphaGaz 2) was used without further purification. NO (AlphaGaz N20) was introduced into the TFR upstream of the tip of the injector after purification by means of ethanol/liquid N_2 cold bath and iron sulfate filter. Typical NO concentration in the TFR was about 4×10^{13} molecules cm^{-3}. A distance from the injector tip to the orifice of the inlet cone of the ion−molecule reactor was fixed at $L = 40$ cm, which corresponded to a reaction time in the TFR of about $t = 30$ ms.

To increase the signal-to-noise ratio of the NO_2 and HNO_3 products of reactions 1a and 1b, a "chemical amplification" was utilized as previously described.[6] CO was added to the TFR to create a reaction chain (1a−2−3) with a chain length of about six

$$OH + CO \rightarrow H + CO_2 \qquad (2)$$

$$H + O_2 + M \rightarrow HO_2 + M \qquad (3)$$

O_2 (AlphaGaz 2) and CO (AlphaGaz N37) were added into the main N_2 stream using CELERITY flow controllers. Typical concentrations were $[O_2] \approx 2 \times 10^{16}$ and $[CO] \approx 5 \times 10^{17}$ molecules cm^{-3}. At the same time, CO acted as a scavenger of OH radicals to prevent formation of nitric acid in the secondary reaction (4)

$$OH + NO_2 + M \rightarrow HNO_3 + M \qquad (4)$$

Water vapor was introduced into the reactor along with the main Ar flow passing through the stainless steel bubbler filled with either distilled H_2O or D_2O (Aldrich, 99.9%). The difference between the saturated vapor pressures of H_2O and D_2O was taken into account when calculating water concentration in the reactor. The bubbler was filled with glass beads in order to prevent water spurting and was kept at a constant temperature of 22 °C. The main N_2 flow was separated into two flows, one of which passed through the bubbler and further joined with the bypass flow. Its fraction could be varied from zero to total N_2 flow, creating in the reactor a variable humidity measured by a high-performance optical dew-point transmitter OPTIDEW (Michell Instruments) inserted into the inlet tube downstream from the joint point of the two N_2 flows. As the readings of this hygrometer were unstable both in the range of low (0−3% relative humidity (rh)) and high (>70% rh) water concentrations, it was replaced by a VAISALA DRYCAP DMT340 dew-point transmitter for a few measurements.

Detection System. The gas mixture from the TFR was sampled through a Teflon cone into the ion−molecule reactor (IMR). The typical pressure in the IMR was about 1 Torr with the flow rate of the Ar carrier gas of about 4 SLPM. The electrons and the primary Ar^+ ions were generated in the ion source with a heated filament. SF_6 was continuously introduced into the IMR downstream of the ion source. The primary SF_6^- negative ions were produced by attachment of the electrons to

Water Vapor Effect on the HNO₃ Yield

J. Phys. Chem. A, Vol. 113, No. 42, 2009 **11329**

TABLE 1: Mass Numbers of Negative Ion Clusters Observed in the Presence of H₂O or D₂O in Ar/SF₆ Afterglow with Addition of Trace Amounts of NO₂ and HNO₃[a]

|	with H₂O						with D₂O				
			ion core						ion core		
ligand	F⁻	OH⁻	NO₂⁻	NO₃⁻	SF₆⁻	ligand	F⁻	OD⁻	NO₂⁻	NO₃⁻	SF₆⁻
	19	17	46	62	146		19	18	46	62	146
(HF)₁	39	37	66	**82**	166	(DF)₁	40	39	67	_*83*_	167
(HF)₂	59	57	86	-		(DF)₂	61	60	88		
(HF)₃	_79_	77				(DF)₃	**82**	81			
(HF)₄	99	97				(DF)₄	103	*102*			
(H₂O)₁	37	35	64	_80_	164	(D₂O)₁	39	38	66	**82**	166
(H₂O)₂	55	53	**82**			(D₂O)₂	59	58	_86_		
(H₂O)₃	73	71				(D₂O)₃	79	78			
(H₂O)₄	91	89				(D₂O)₄	99	98			

[a] Boldface numbers correspond to the clusters interfering with the ions of the reaction products. Underlined numbers are the isotopic homologues for the interfering clusters. Italics denote the clusters interfering with the products of the ion−molecule reaction 3i (see text).

SF₆. NO₂ and HNO₃ were detected as NO₂⁻ (*m/e* 46) and F⁻·HNO₃ (*m/e* 82) ions formed, respectively, by electron and fluorine transfer from SF₆⁻:[19]

$$SF_6^- + NO_2 \rightarrow NO_2^- + SF_6 \qquad (1i)$$

$$SF_6^- + HNO_3 \rightarrow F^- - HNO_3 + SF_5 \qquad (2ia)$$
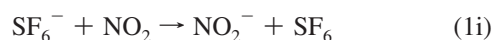
Although the most probable structure of the ion formed in reaction 2ia is NO₃⁻·HF that corresponds to potential energy minimum, we denote it as F⁻·HNO₃ in order to distinguish the origin of this ion from the NO₃⁻·HF cluster formed by addition of HF to NO₃⁻ ion (vide infra). The formed ions entered the mass analyzer through a 180 μm orifice in the nickel skimmer representing the first element of the ion optics. After passing the quadrupole mass analyzer (EXTREL), the ions were registered in the ion counting mode using a Channeltron multiplier and a MTS-100 preamplifier. The detection limits (2σ S/N, 50s) were 6 × 10⁹ molecules cm⁻³ for NO₂ and 7 × 10⁸ molecules cm⁻³ for HNO₃.

In addition to the primary SF₆⁻ ion, the fragment ions F⁻ (*m/e* 19), SF₃⁻ (*m/e* 89), SF₄⁻ (*m/e* 108) and SF₅⁻ (*m/e* 127) were always present in the negative background mass spectrum. Mechanisms of their formation have been discussed in the studies of corona and glow discharges in SF₆.[18−20] In particular, reaction 3i was recognized as one of the sources of SF₅⁻ ions, at the same time giving rise to peaks at *m/e* 83 and 102[19−21]

$$SF_6^- + SO_2 \rightarrow F^- - SO_2, F_2^- \cdot SO_2, SF_5^- \qquad (3i)$$
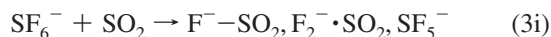
This reaction takes place owing to the formation of reactive neutral species SF₄ and SF₂, which presumably react with O₂ and H₂O traces producing SO₂.[20] Increase of water concentration favors production of SO₂ resulting in an increase of signal intensities at masses 83 (F⁻·SO₂) and 102 (F₂⁻·SO₂).[22] Below, we consider other important processes in the IMR caused by elevated water concentrations.

Influence of Water on Detection Processes. The important consequence of the water presence in the IMR is a decrease of the intensities of the signals corresponding to the primary F⁻ and SF$_x$⁻ ions (*x* = 3−6). Also, new ions appear due to clustering and ion−molecule reactions with H₂O. Our observations were in agreement with the results of the study of the water effect on the negative mass spectra in pure SF₆ discharge.[22]

In our study, mass spectra indicate formation of the clusters X⁻·(HF)$_n$ and X⁻·(H₂O)$_n$, where X⁻ is the ion core (X = F, OH) and *n* = 0−4. At maximum H₂O concentration of 6 × 10¹⁷ molecules cm⁻³ (80% rh) in the TFR corresponding to about 2 × 10¹⁴ molecules cm⁻³ in the IMR, the F⁻ and OH⁻ water clusters peaked for *n* = 3, while their HF clusters peaked for *n* = 2. The SF₆⁻·HF and SF₆⁻·H₂O clusters with one ligand were also observed. Similar clusters were observed in the presence of D₂O. It is worth noting that the observed cluster size distribution was affected by declustering processes behind the sampling cone and did not correspond to the equilibrium distribution at the IMR temperature. The mass numbers of the observed ion clusters in the presence of H₂O and D₂O are collected in Table 1. Even a low water concentration (below the OPTIDEW hygrometer sensitivity limit) resulted in a drop of SF₆⁻ ion signal intensity accompanied by a sharp increase of the OH⁻ signal intensity. The latter can be explained by the formation of OH in the fast reaction between the neutral species in the IMR, followed by OH ionization[23]

$$F + H_2O \rightarrow OH + HF \qquad (4i)$$

$$SF_6^- + OH \rightarrow OH^- + SF_6 \qquad (5i)$$
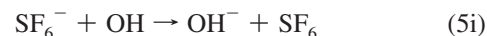
Also, reaction with water was suggested as a likely source of OH⁻[22]

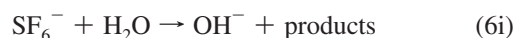$$SF_6^- + H_2O \rightarrow OH^- + products \qquad (6i)$$

Figure 2 shows the intensities of the SF₆⁻, OH⁻, and F⁻·SO₂ ions as a function of relative humidity in the TFR. To avoid signal saturation, the SF₆⁻ ion was monitored at the peak of ³⁴SF₆⁻ natural isotope (3.6%) at *m/e* 148. Effective clustering with H₂O and HF explains a further decrease of OH⁻ ion concentration with the increase of water content. The decrease of SF₆⁻ intensity can be partly explained by the cluster-mediated reactions between SF₆⁻ and H₂O[24,25]
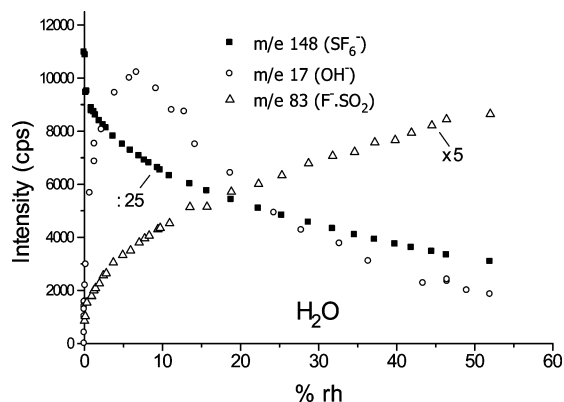
$$SF_6^- + H_2O \rightarrow SF_6 - \cdot H_2O \qquad (7i)$$
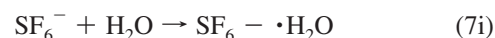
Figure 2. Typical dependence of the intensity of primary SF_6^- ions and background OH^- and $F^- \cdot SO_2$ ions on relative humidity in the TFR.

$$SF_6^- \cdot H_2O + H_2O \rightarrow SF_4^- \cdot O, F^- \cdot (HF)_2 \qquad (8i)$$

Reaction 8i is relatively slow and the observed product intensity at *m/e* 124 ($SF_4^- \cdot O$) was much less than the intensity drop at *m/e* 146 (SF_6^-). Another cause of the SF_6^- decay can be the increased recombination and wall losses due to the increased rate of the ambipolar diffusion. Since the OH^- and $F^- \cdot SO_2$ ions are produced presumably by the reactions involving SF_6^-, their intensities are presented in Figure 2 as normalized to the SF_6^- signal. Complication of the CIMS mass spectra at high water concentrations of ambient air is a well-known problem in atmospheric measurements of nitric acid.[24,26] To solve this problem, in particular, the reaction

$$SiF_5^- + HNO_3 \rightarrow SiF_5^- \cdot HNO_3 \qquad (9i)$$
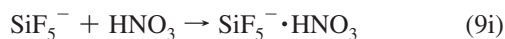
has been suggested to detect HNO_3 in open air.[27] However, in our previous work,[7] it was determined that under our conditions in the IMR, the detection scheme with the use of reaction 9i was about 20 times less efficient compared to that with reaction 2ia and inapplicable for systematic measurements. This detection method was tested again during the present study, but it gave a detection limit that was too high, 6×10^9 molecules cm^{-3} (2σ S/N, 100 s), that did not allow us to reliably measure the signal under dry conditions. The HNO_3 detection limit, using SF_6^- as a primary ion in reaction 2ia, depended on humidity because of both the increase of the background signal and decrease of concentration of the ionizing ion. It was increasing by approximately a factor of 3 at 50% rh compared to dry conditions, giving at this humidity a value of 1.8×10^9 molecules cm^{-3} (2σ S/N, 50 s).

The major product of reaction 1a is NO_2, which can give products other than the NO_2^- ion in the presence of water in the IMR. The only other species, except NO_2 and minor HNO_3 product, observed in the negative mass-spectrum in the course of reaction 1a in the TFR were OH and HO_2. The stationary concentrations of OH and HO_2 were rather low and their reactions with SF_6^- giving OH^- (*m/e* 17) and $SF_4O_2^-$ ions (*m/e* 140)[28] were not important in the present study
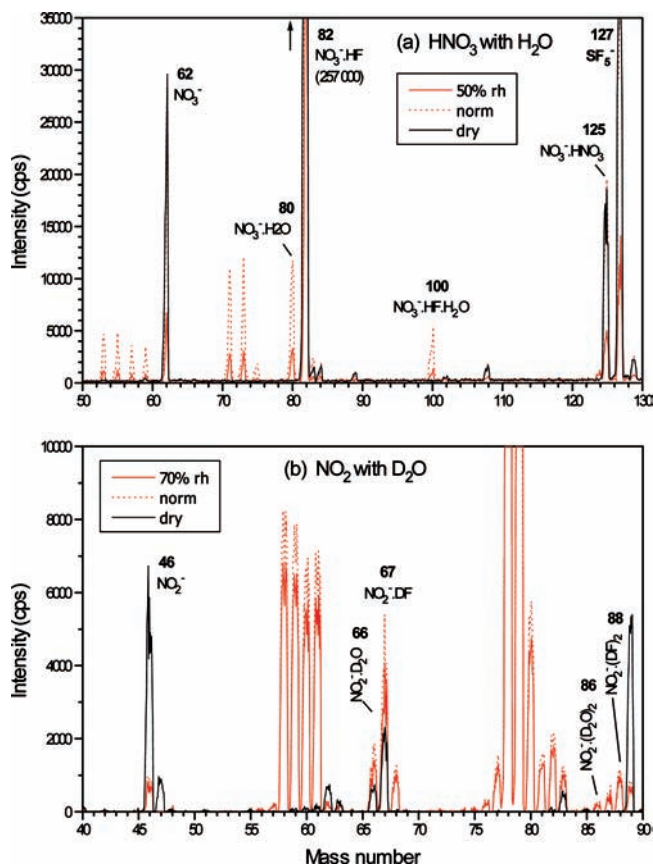
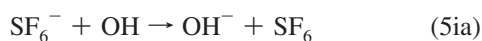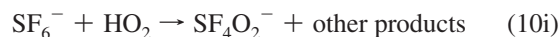$$SF_6^- + OH \rightarrow OH^- + SF_6 \qquad (5ia)$$

Figure 3. Mass spectra of HNO_3 (a) and NO_2 (b) in the presence of H_2O and D_2O, respectively. Black lines correspond to dry conditions; solid red lines correspond to raw mass spectra in humid conditions; dotted red lines are the humid mass spectra after normalization by the SF_6^- peak intensity.

$$SF_6^- + HO_2 \rightarrow SF_4O_2^- + \text{other products} \qquad (10i)$$

Accordingly, only the negative spectra of NO_2 and HNO_3 in the presence of H_2O and D_2O had to be examined to assess the contribution of peaks with *m/e* 82 interfering with the HNO_3 product from reaction 1a. As the concentration of the primary negative SF_6^- ion decreased in the presence of water, corresponding corrections were made when comparing signals at different H_2O concentrations. Namely, the signal intensities for all the ions presumably originating from the reactions with SF_6^- were normalized by the SF_6^- ion intensity.

Figure 3a presents HNO_3 spectra registered when gaseous HNO_3 was introduced into the TFR along with He flow bubbling through the mixture of concentrated nitric and sulfuric acids. Concentration of HNO_3 in the reactor during these measurements was about 8×10^{12} molecules cm^{-3} as calculated from the assumption that the He flow was saturated by HNO_3 vapor. In the absence of water, the HNO_3 spectrum consists of three peaks: *m/e* 62 (NO_3^-), *m/e* 82 ($F^- \cdot HNO_3$), and *m/e* 125 ($NO_3^- \cdot HNO_3$). The two latter can be considered as stable association complexes.[29] The NO_3^- ion is a coproduct of reaction 2ia with the estimated yield of about 6%[19]

$$SF_6^- + HNO_3 \rightarrow NO_3^- + \text{other products} \qquad (2ib)$$
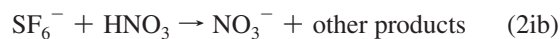
In the spectrum of Figure 3a its peak intensity is about 11% of the main peak intensity at *m/e* 82. In the presence of H_2O, the

Water Vapor Effect on the HNO₃ Yield

J. Phys. Chem. A, Vol. 113, No. 42, 2009 **11331**

$NO_3^- \cdot H_2O$ (*m/e* 80) and $NO_3^- \cdot H_2O \cdot HF$ (*m/e* 100) clusters originating from HNO₃ were observed in addition to the above-mentioned ions. The $NO_3^- \cdot H_2O$ cluster is formed rather by H_2O addition to NO_3^- (11i) than by ligand substitution reaction (12i)

$$NO_3^- + H_2O \rightarrow NO_3^- \cdot H_2O \qquad (11i)$$

$$NO_3^- \cdot HF + H_2O \rightarrow NO_3^- \cdot H_2O + HF \qquad (12i)$$
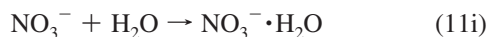
as reaction 12i is probably endothermic and is not expected to be fast.[26,29] Therefore, only formation of the mixed $NO_3^- \cdot H_2O \cdot HF$ cluster could affect measurements of HNO₃ intensity at *m/e* 82. However, the relative peak intensity of this cluster with respect to the intensity at *m/e* 82 is about 2% only, which allows us to neglect its influence on HNO₃ intensity. Figure 4a shows that the intensities of the peaks at *m/e* 82 (open squares) and *m/e* 148 (stars) decrease in the presence of water vapor. The standard deviations of these signal intensities are less than the symbol size. At the same time, the HNO₃ peak intensity normalized by SF_6^- signal intensity (*m/e* 82, filled squares) remains nearly constant when relative humidity in the TFR changed from zero to 70%. The 2σ error bars include the signal and normalization deviations. A slight increase at low water concentration can be explained by reaction 13i

$$NO_3^- + HF \rightarrow NO_3^- \cdot HF \qquad (13i)$$
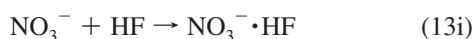
In general, it can be concluded that the normalized HNO₃ signal at *m/e* 82 does not depend on water concentration within experimental error.
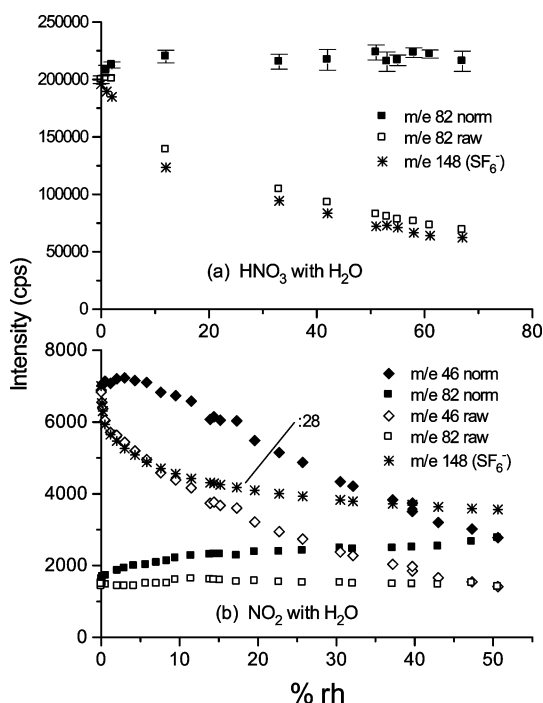

Figure 4. (a) Humidity dependence of HNO₃ intensity (2σ level) with HNO₃ concentration in the TFR of approximately 8×10^{12} molecules cm⁻³. Signal at *m/e* 82 consists of $F^- \cdot HNO_3$ and $NO_3^- \cdot HF$ ions. (b) Humidity dependence of NO₂ intensity (*m/e* 46) and combined signal intensity at *m/e* 82 consisting of contributions from HNO₃ ($F^- \cdot HNO_3$) and from $NO_3^- \cdot HF$ and $NO_2^- \cdot (H_2O)_2$ clusters. NO₂ concentration in the TFR was 3×10^{12} molecules cm⁻³.

When NO₂ was introduced into the TFR (commercial 0.5% mixture in N₂, Air Liquide), formation of HF and H₂O clusters with NO_2^- and NO_3^- ion cores was observed as shown in Figure 3b. The NO_3^- clusters were formed due to the HNO₃ impurity in the NO₂ mixture, giving NO_3^- ion in reaction 2ib, with a partial contribution from the background NO_3^- ions. The observed NO_2^- clusters were $NO_2^- \cdot (HF)_n$ and $NO_2^- \cdot (H_2O)_n$ ($n = 1, 2$). The $NO_2^- \cdot (H_2O)_2$ cluster with mass 82 interferes with both $NO_3^- \cdot HF$ cluster and $F^- \cdot HNO_3$ ion from nitric acid. Figure 4b shows the humidity dependence of the normalized intensities at *m/e* 46 and 82 for NO₂ concentration of 3×10^{12} molecules cm⁻³. The signal at *m/e* 46 represents NO_2^-, and its decrease is explained by efficient clustering (vide infra). Initial growth of the NO_2^- intensity peaked at about (5−7)% rh can be explained by the charge exchange reaction with OH^- ions

$$OH^- + NO_2 \rightarrow NO_2^- + OH \qquad (14i)$$
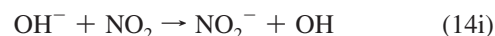
with a rate constant more than an order of magnitude higher than that of reaction 1i.[23] The signal at *m/e* 82 consists of the contributions from the HNO₃ impurity, $F^- \cdot HNO_3$ and $NO_3^- \cdot HF$, and $NO_2^- \cdot (H_2O)_2$ clusters. A detailed examination of NO₂ mass spectra in the presence of water vapor showed that the consumption of NO_2^- ion corresponded to formation of the NO_2^- ion clusters. For example, the spectrum of NO₂ in the presence of D₂O showed that a major part of NO_2^- ions was consumed in reactions forming $NO_2^- \cdot DF$ (*m/e* 67) and $NO_2^- \cdot D_2O$ (*m/e* 66) clusters with a smaller part consumed in reactions forming $NO_2^- \cdot (D_2O)_2$ (*m/e* 86) and $NO_2^- \cdot (DF)_2$ (*m/e* 88) clusters (Figure 3b).

Also, it is necessary to mention the possibility of heterogeneous hydration of NO₂ giving HONO and HNO₃ that might take place on the walls of the TFR, IMR, or interfaces according to the following reaction equation

$$2NO_2(g) + H_2O(s) \rightarrow HONO(g) + HNO_3(s,g) \qquad (5)$$

A detailed mechanism was investigated by Finlayson-Pitts with co-workers.[30,31] Until recently it was believed that HNO₃ does not leave the surface unlike HONO which goes to the gas phase,[30] but in a more recent study, HNO₃ has been detected in the gas phase by FTIR.[31] However, the time scale of reaction 5 was about 10 h for 30% consumption of NO₂ at 51% relative humidity,[31] which exceeds by many orders of magnitude the time scale of the practically "immediate" response of NO₂ and HNO₃ signals to the introduction of water in our experiments. This indicates that the wall effects described by reaction 5 do not play any noticeable role in our study. The absence of influence of the reactor walls was also checked by introducing NO₂ through the movable injector, when the signals at *m/e* 46 and 82 did not change with the change of the position of the injector at different H₂O concentrations from 0 to 3×10^{17} molecules cm⁻³. Additional evidence for the absence of influence of wall effects on the behavior of the peak at *m/e* 82 is the absence of hysteresis in the observed water dependences. Humidity-related hysteresis is typical for products of wall reactions and was observed, for example, for NO_3^- and $F^- \cdot SO_2$ ions. It can be explained by the fact that a surface water layer remains on the walls for a relatively long time after stopping the water vapor flow through the reactor.

II.2. Experimental Results. In the previous studies, the branching ratio of reaction 1a, $\beta = k_{1b}/k_{1a}$, was obtained by measuring the concentration ratio of the HNO₃ and NO₂ products
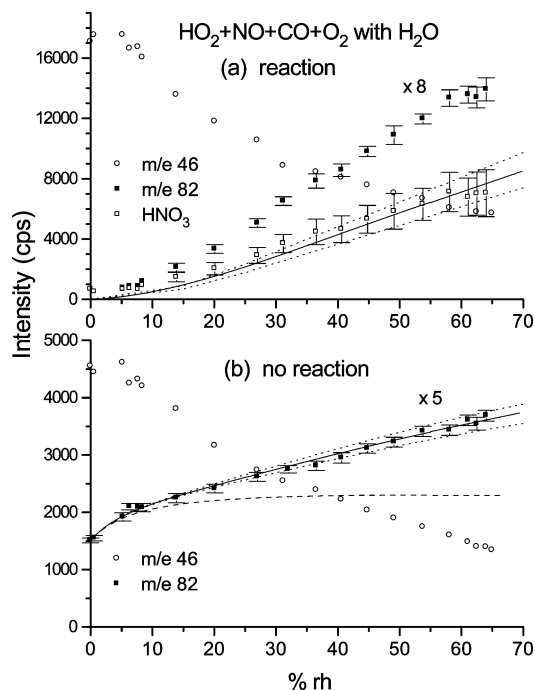
Figure 5. Typical signal intensities in the $HO_2 + NO + O_2 + CO + H_2O$ system as a function of relative humidity in the TFR. (a) Reaction (discharge on−off): NO_2 product (*m/e* 46) and combined signal from HNO_3 product and $NO_2^- \cdot (H_2O)_2$ cluster (*m/e* 82); solid curve is the cluster contribution determined as described in the text and open squares correspond to the net HNO_3 reaction product signal. (b) No reaction (discharge off): NO_2 impurity (*m/e* 46) and combined signal from HNO_3 impurity and $NO_3^- \cdot HF$ and $NO_2^- \cdot (H_2O)_2$ clusters (*m/e* 82). The latter is fitted by the solid curve which is a sum of the scaled $NO_3^- \cdot HF$ (dashed curve) and the $NO_2^- \cdot (H_2O)_2$ humidity functions (see text). Dotted curves show error limits.

from channels 1b and 1a, respectively.[6,7] In the present work, water vapor concentration was varied at a fixed injector position, which means that NO_2 concentration produced in reaction 1a was constant, which is valid since $\beta \ll 1$. Water effect was determined by measuring the relative change of nitric acid concentration with changing H_2O concentration in the TFR. In each experiment, water concentration dependences of the signals at *m/e* 46, *m/e* 82, and *m/e* 148 were measured with discharge on and off. The difference between the discharge on and discharge off signal intensities corresponded to NO_2 and HNO_3 produced in the $HO_2 + NO$ reaction. Typical humidity dependence is shown in the top panel of Figure 5 (2σ error bars include normalization error). The initial reactant concentrations for this measurement are indicated in the upper line of Table 2 (experiment 1). The signal at *m/e* 46 corresponds to the formed NO_2 and it decreases with humidity due to NO_2^- clustering. The signal at *m/e* 82 is a combined signal of $F^- \cdot HNO_3$ from the formed HNO_3 and $NO_2^- \cdot (H_2O)_2$ ion cluster from NO_2 formed in the reaction

$$I_{82}^R(rh) = I_{HNO_3}^R(rh) + I_{NO_2(H_2O)_2}^R(rh) \qquad (E1)$$

Water dependence of the signal $I_{HNO_3}^R$ can be determined by subtraction of the cluster contribution from the total intensity at *m/e* 82. The cluster contribution was derived from the water dependence of the signal at *m/e* 82, without discharge, I_{82}^0 (Figure 5b). Signal I_{82}^0 measured in the absence of reaction is from the NO_2 and HNO_3 trace impurities in NO ($NO_2^- \cdot (H_2O)_2$ and $F^- \cdot NO_3$ ions, respectively) and from the background NO_3^- ions

($NO_3^- \cdot HF$ clusters). We can write

$$I_{82}^0(rh) = I_{HNO_3}^0(rh) + I_{NO_3HF}^0(rh) + I_{NO_2(H_2O)_2}^0(rh) \qquad (E2)$$

where $I_{HNO_3}^0$ is the water independent contribution from the HNO_3 impurity, $I_{NO_3HF}^0$ is the water dependent contribution from the background NO_3^-, and $I_{NO_2(H_2O)_2}^0$ is the water dependent interference from the NO_2 impurity. In independent experiments it was found that the humidity dependences of the $I_{NO_2(H_2O)_2}^0(rh)$ signal can be represented as

$$I_{NO_2(H_2O)_2}^0(rh) = C_1 I_{46}^0 [NO_2]^0 f_{NO_2(H_2O)_2} \qquad (E3)$$

where C_1 is the water independent coefficient, constant for a given experiment, I_{46}^0 is the NO_2 signal in the absence of water, corresponding to NO_2 concentration in the TFR without reaction, and $f_{NO_2(H_2O)_2}$ is the function, which depends only on the H_2O concentration in the TFR. Coefficient C_1 can change from one experiment to another due to the changes in the parameters of the ion optics, pressure, or flow conditions. It was also found that the contribution from the NO_3^- ion can be expressed in a similar form, as a product of water independent coefficient and a function, describing the shape of water dependence

$$I_{NO_3HF}^0(rh) = C_2 f_{NO_3HF}(rh) \qquad (E4)$$

As a result, the signal at *m/e* 82 without discharge can be written as a sum of two functions of different shapes:

$$I_{82}^0(rh) = C_0 + C_1 I_{46}^0 f_{NO_2(H_2O)_2}(rh) + C_2 f_{NO_3HF}(rh) \qquad (E5)$$

The C_0, C_1, and C_2 coefficients were derived by least-squares fitting of the experimental $I_{82}^0(rh)$ dependence and the obtained C_1 coefficient was used to determine the HNO_3 signal intensity from the reaction

$$I_{HNO_3}^R(rh) = I_{82}^R(rh) - C_1 I_{46}^R f_{NO_2(H_2O)_2}(rh) \qquad (E6)$$

where I_{46}^R is the NO_2 signal intensity in the absence of water, corresponding to NO_2 concentration in the TFR produced by the reaction. In the three next paragraphs the determination of the humidity functions $f_{NO_2(H_2O)_2}(rh)$ and $f_{NO_3HF}(rh)$ is described.

Formation of the $NO_2^- \cdot (H_2O)_2$ water cluster was examined in special measurements by flowing NO_2 and D_2O into the reactor. In this case, $NO_2^- \cdot (D_2O)_2$ could be detected at a pure *m/e* 86 peak without any interference. Figure 6 shows a typical humidity dependence of its formation which can be fitted by a polynomial function $f_{NO_2(H_2O)_2} = a_1 x + b_1 x^2 + c_1 x^3$ represented by a solid line, where x is the relative humidity (%) in the TFR. It was checked for several D_2O concentrations (corresponding to 9%, 16%, and 40% rh) that the intensity of the $NO_2^- \cdot (D_2O)_2$ cluster was directly proportional to NO_2 concentration in the TFR. Figure 7 shows the results of such measurements at 40% rh in the NO_2 range up to 5.5×10^{12} molecules cm^{-3} covering the range between the background and the total NO_2 concentration produced in reaction 1a. This allows us to quantify the

TABLE 2: Water Enhancement Factor of the HNO₃ Yield, f_{hum}, at 50% Relative Humidity

exp no.	[NO] (10^{13})	[CO] (10^{17})	[O₂] (10^{16})	chain length	$C_{148}{}^a$	[HO₂]₀ (10^{11})	$\Delta[NO_2]^b$ (10^{12})	$\Delta[HNO_3]^b$ (10^9)	$I_{HNO_3}^{R(0\%rh)}$ (cps)	$I_{HNO_3}^{R(50\%rh)}$ (cps)	f_{hum}
1	4.9	5.1	1.9	6.4	0.88	3.4	2.1	2.3	86 ± 13	675 ± 160	7.9 ± 2.2
2	4.9	5.1	1.9	6.4	0.93	5.3	3.4	4.1	95 ± 4	776 ± 170	8.2 ± 1.7
3	3.8	4.9	1.7	4.3	0.89	4.4	1.9	3.2	68 ± 3	469 ± 99	6.9 ± 1.8
4	4.1	3.8	1.6	6.0	0.72	3.3	2.0	3.1	83 ± 10	623 ± 157	7.5 ± 2.0

^{a} Normalization coefficient, $C_{148} = I_{148}(50\%rh)/I_{148}(0\%rh)$, is the ratio of SF_6^- ion intensities with and without water. ^{b} Product concentrations in the absence of water; concentrations are in units of molecules cm⁻³.
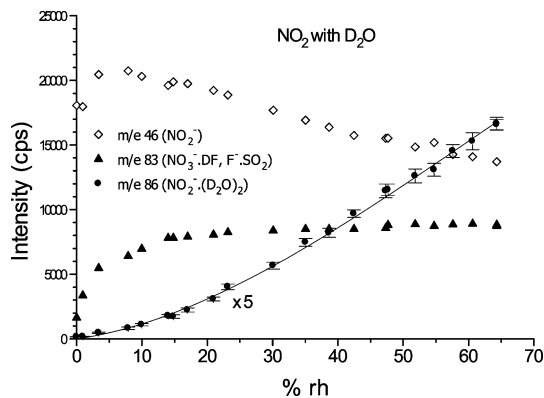

Figure 6. Humidity dependence of NO_2^- (*m/e* 46) and $NO_2^- \cdot (D_2O)_2$ cluster (*m/e* 86) ion intensities. NO₂ concentration in the TFR was 3.5 × 10¹² molecules cm⁻³. Signal at *m/e* 83 belongs mainly to $NO_3^- \cdot DF$ cluster with a minor contribution of $F^- \cdot SO_2$.
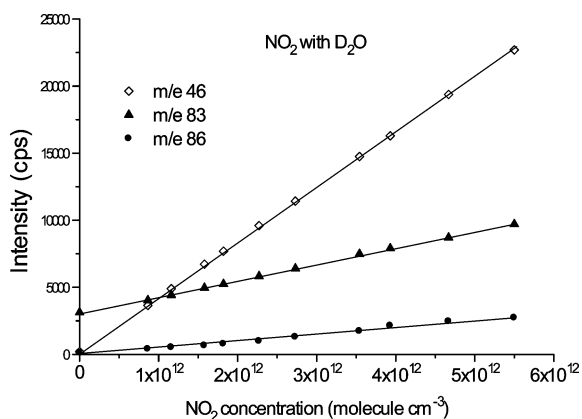

Figure 7. Dependence of the ion intensities presented in Figure 6 on NO₂ concentration at D₂O relative humidity of 40%.
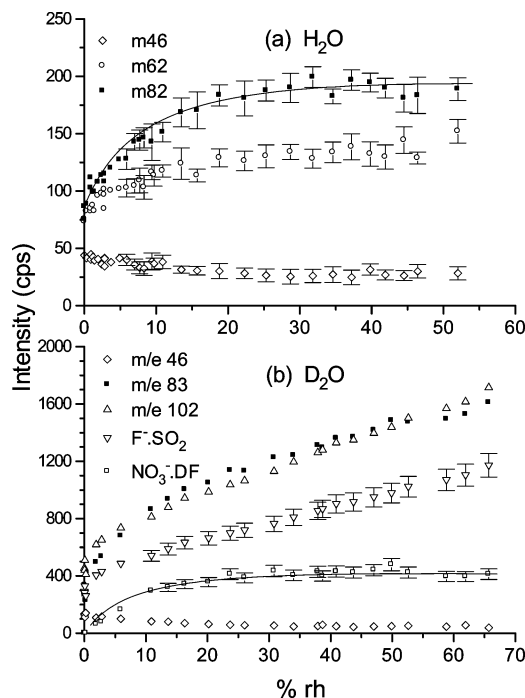

Figure 8. Humidity dependence of the background signal intensities with H₂O (a) and D₂O (b). Down triangles present the $F^- \cdot SO_2$ contribution to the signal at *m/e* 83. Solid curves represent generic humidity function for the $NO_3^- \cdot HF$ cluster.

cluster contribution to the reaction signal as the $NO_2^- \cdot (H_2O)_2$ signal in the absence of the reaction scaled by NO₂ concentration.

The $NO_3^- \cdot (HF)$ cluster cannot be studied simply by using its $NO_3^- \cdot (DF)$ deutero homologue, since the latter interferes at *m/e* 83 with the water dependent $F^- \cdot SO_2$ ion from reaction 3i. We measured water dependence for $NO_3^- \cdot (HF)$ cluster with flowing only H₂O into the reactor, after minimization of NO₂ background. The result is shown in the top panel of Figure 8. The curve at *m/e* 82 represents the $NO_3^- \cdot (HF)$ cluster formed from the background NO_3^- ion. The NO_3^- ion intensity (*m/e* 62) slightly increases when water is introduced into the TFR and is maintained at its maximum value after stopping the water supply. This indicates that the background NO_3^- ion is formed in wall reactions with participation of H₂O adsorbed on the surface in the IMR. In Figure 8a, the contribution of $NO_2^- \cdot (H_2O)_2$ to the signal at *m/e* 82 was negligible.

Another way to obtain humidity curves for $NO_3^- \cdot HF$ was to separate the $NO_3^- \cdot DF$ and $F^- \cdot SO_2$ contributions at *m/e* 83 in experiments with D₂O, taking into account that $F^- \cdot SO_2$ intensity

does not depend on NO₂ concentration. Water dependence for $F^- \cdot SO_2$ could be obtained using the peak at *m/e* 83 with H₂O (see Figure 2) or the peak at *m/e* 102 with D₂O. The latter belongs to the $F_2^- \cdot SO_2$ ion from the same reaction 3i as $F^- \cdot SO_2$ and, hence, is expected to exhibit the same behavior. The background intensities for both $F^- \cdot SO_2$ and $F_2^- \cdot SO_2$ ions were increasing with addition of O₂, but the average ratio $I_{83}/I_{102} = 0.65 \pm 0.04$ was constant during the whole period of measurements. This ratio is in agreement with the preferable formation of $F_2^- \cdot SO_2$ ion in (3i) found in ref 19. Figure 8b demonstrates the extraction of the $NO_3^- \cdot DF$ signal from the signal measurements at *m/e* 83 and 102 with D₂O, practically, in the absence of NO₂. Solid squares and up triangles represent raw measurements at *m/e* 83 (combined $F^- \cdot SO_2$ and $NO_3^- \cdot DF$ signal) and *m/e* 102 ($F_2^- \cdot SO_2$), respectively; down triangles are the scaled $F_2^- \cdot SO_2$ signal representing $NO_3^- \cdot DF$ contribution to *m/e* 83; open squares are the difference between the total intensity at *m/e* 83 and $F_2^- \cdot SO_2$ contribution, representing humidity behavior of the $NO_3^- \cdot DF$ cluster. This behavior could be fitted by the analytical function $f_{NO_3HF}(rh) = a_2 x/(b_2 + x) - c_2 x$, where a_2, b_2, and c_2 are constants and x is the relative humidity (%) in the TFR. The $NO_3^- \cdot DF$ humidity curves calculated using this expression are presented in parts a and b of Figure 8 by solid lines.

Having obtained the $NO_2^- \cdot (H_2O)_2$ and $NO_3^- \cdot (HF)$ humidity curve shapes, the complex signal at *m/e* 82 in the absence of

reaction was deconvoluted following eq E5 as illustrated in Figure 5b. At first, the C_0 and C_2 coefficients from (E4) were fitted ($NO_3^- \cdot HF$ contribution, dashed curve), then the $NO_2^- \cdot (H_2O)_2$ component was added by fitting C_1 from (E3) to obtain the total $I_{82}^0(rh)$ (solid curve). The dotted curves show the error limits for $NO_2^- \cdot (H_2O)_2$ contribution corresponding to 12% variation of C_1. Then, the cluster contribution to the reaction signal at m/e 82, $I_{NO_2(H_2O)_2}^R(rh)$, was calculated, according to the NO_2 signal I_{46}^R. The $I_{NO_2(H_2O)_2}^R(rh)$ dependence is represented in Figure 5a by a solid curve. The dotted curves correspond to the uncertainty limits imposed by fitting ($\approx$14%). Finally, the net HNO_3 signal from the reaction, $I_{HNO_3}^R(rh)$, was obtained using eq E6 (open squares in Figure 5a). In Figure 5a, the HNO_3 concentration increases from $I_{HNO_3}^R(0\%rh) = 85 \pm 13$ cps to $I_{HNO_3}^R(50\%rh) = 675 \pm 160$ cps giving a factor of 7.9 ± 2.2.

The results of four similar experiments are presented in Table 2. Figure 5 shows the signals from experiment 1. Experiment 2 was conducted over the same conditions but slightly lower Ar flow through the IMR. Experiment 3 was carried out with lower NO concentration, and experiment 4 with lower initial HO_2 concentration. The estimated upper limit for the HNO_3 contribution from reaction 4 into the $I_{HNO_3}^R(0\%rh)$ was less than 10% in all four experiments. The last column in Table 2 presents an enhancement factor, f_{hum}, at 50% relative humidity ($[H_2O] \approx 3.9 \times 10^{17}$ molecules cm^{-3}). Enhancement factor is determined as a relative branching ratio, $f_{hum}(rh) = \beta_{hum}(rh)/\beta(0\%rh) = I_{HNO_3}^R(rh)/I_{HNO_3}^R(0\%rh)$, and is calculated as the ratio of the HNO_3 signal intensities under humid and dry conditions. An average enhancement factor of $f_{hum}(50\%rh) = 7.6 \pm 1.5$ is obtained from four experiments, giving $\beta_{hum}(50\%rh) = 1.3\%$ at 298 K and 200 Torr. Error limits are mainly determined by the uncertainty of the cluster contribution to the reaction signal at m/e 82. Varying the possible limits for the $NO_2^- \cdot (H_2O)_2$ contributions like in Figure 5b, this uncertainty was about 20% in all the experiments. With addition of the experimental errors in the measurement of low signal intensities of the HNO_3 reaction product under dry conditions, the total uncertainty for f_{hum} is about 30%. Full humidity dependences $f_{hum}(rh)$ from all the experiments are plotted in Figure 9a.

II.3. Discussion. *Reaction Mechanism.* The enhancement of HNO_3 formation yield in reaction 1a in the presence of water vapor can be explained by the formation of the hydrogen bonded $HO_2 \cdot H_2O$ complex

$$HO_2 + H_2O \leftrightarrow HO_2 \cdot H_2O \qquad (6)$$
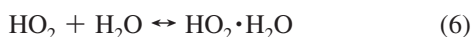
This complex has been observed experimentally,[32,33] and its existence was confirmed by quantum-mechanical calculations.[34] Formation of this complex has been used to explain the kinetics of the HO_2 self-reaction in the presence of H_2O.[1–5] For example, Kanno et al.[2] found that the rate constant of the HO_2 self-reaction increased approximately by a factor of 2 in the presence of water at 50% rh. From their measurements they derived the equilibrium constant, $K_6 = (5.2 \pm 3.2) \times 10^{-19}$ cm^3 molecule^{-1} at 298 K, and, assuming the water enhancement mechanism with formation of the $HO_2 \cdot H_2O$ complex and its rapid reaction, they obtained the rate constant of the $HO_2 + HO_2 \cdot H_2O$ reaction. The latter appeared to be 1 order of magnitude higher than the rate constant of the $HO_2 + HO_2$ reaction.

A similar mechanism can be expected for the HO_2 reaction with NO, where NO reacts with the $HO_2 \cdot H_2O$ complex

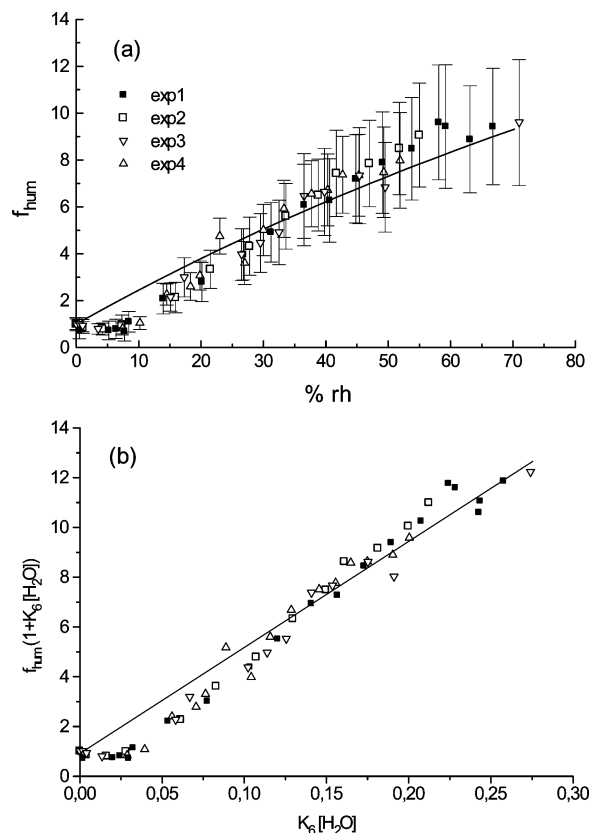$$HO_2 \cdot H_2O + NO \rightarrow OH + NO_2 + H_2O \qquad (1aw)$$

Figure 9. Water effect on the HNO_3 yield in $HO_2 + NO$ reaction. (a) Enhancement factor, $f_{hum} = \beta_{hum}/\beta$, as a function of relative humidity in the TFR. Solid curve is the calculation assuming the mechanism described in the text with $k_{1bw}/k_{1b} = 42$. (b) Linearized plot for determination of β_w/β.

$$HO_2 \cdot H_2O + NO \rightarrow HNO_3 + H_2O \qquad (1bw)$$

In an earlier study, Bohn and Zetzsch found that the total rate constant of the $HO_2 + NO$ reaction did not depend on water concentration with $[H_2O] = 3.6 \times 10^{17}$ molecules cm^{-3} (53%rh) at room temperature and pressures of 75, 375, and 750 Torr.[35] As well, the OH yield (>95%) did not change with water within the 5% accuracy of their experiments. It means that $\beta_{hum} \leq 0.05$, and, since at 298 K and 53% rh about 20% of HO_2 radicals are present in the form of complex with H_2O, it means that the complex formation does not change noticeably the rate constant of the main channel, i.e., $k_{1a} \approx k_{1aw}$. This supports the assumption of a negligible change of the NO_2 product yield made in our HNO_3 yield measurements in the presence of H_2O. It is then the increase of the specific branching ratio, $\beta_w = k_{1bw}/k_{1aw}$, in the NO reaction with the $HO_2 \cdot H_2O$ complex, which is responsible for the increase of the HNO_3 yield in the presence of H_2O. Therefore, β_w can be derived from the measured enhancement factor as a function water concentration. If the initial HO_2 concentration without water is $[HO_2]_0$, a part of it appears in the form of complex with addition of water

$$[HO_2]_0 = [HO_2 \cdot H_2O] + [HO_2] \qquad (E7)$$

$$[HO_2 \cdot H_2O] = K_6[H_2O][HO_2] \qquad (E8)$$

From these two equations, $[HO_2] = [HO_2]_0/(1 + K_6[H_2O])$. Let us define the effective (observed) branching ratio in the

Water Vapor Effect on the HNO₃ Yield

J. Phys. Chem. A, Vol. 113, No. 42, 2009 **11335**

presence of water as earlier, $\beta_{hum} = [HNO_3]/[NO_2]$. Taking into account that the HNO₃ yield is always much less than unity and $k_{1a} \approx k_{1aw}$, we can write

$$\beta_{hum} = (\beta[HO_2] + \beta_w[HO_2 \cdot H_2O])/[HO_2]_0 = (\beta + \beta_w K_6[H_2O])/(1 + K_6[H_2O]) \quad \text{(E9)}$$

The effective branching ratio can be also expressed in terms of the enhancement factor f_{hum} as $\beta_{hum} = f_{hum} \cdot \beta$. Then, the final expression for f_{hum} takes the form

$$f_{hum} = \beta_{hum}/\beta = (1 + K_6[H_2O]\beta_w/\beta)/(1 + K_6[H_2O]) \quad \text{(E10)}$$

The value of the β_w/β ratio can be easily obtained as a slope of the experimental plot of $f_{hum}(1 + K_6[H_2O])$ vs $K_6[H_2O]$ presented in Figure 9b. The dependence in Figure 9b is close to a linear function with some deviation from linearity at low humidity. This deviation may result from humidity measurement errors at low concentrations of water vapor. Linear fitting constrained by the condition $f_{hum} = 1$ at $[H_2O] = 0$ gives $\beta_w/\beta = 42 \pm 2$, where the indicated uncertainty corresponds to 2σ of fitting only. The humidity dependence for the enhancement factor calculated with this value is also shown in Figure 9a. Taking into account that $k_{1a} \approx k_{1aw}$, the β_w/β ratio is equal to the rate constants ratio k_{1bw}/k_{1b}, indicating that the rate constant for the HNO₃ formation in the reaction of NO with the $HO_2 \cdot H_2O$ complex is more than 40 times higher than that of the reaction with the HO_2 free radical. The branching ratio in the presence of water molecule becomes $\beta_w = k_{1bw}/k_{1aw} \approx 7\%$ and, taking into account the experimental uncertainties in the determination of f_{hum}, the derived rate constant of reaction 1bw is $k_{1bw} = (6 \pm 2) \times 10^{-13}$ cm³ molecule⁻¹ s⁻¹ at 298 K and 200 Torr.

Implication for Chemical Amplifiers. The present value of k_{1b} can be compared with the rate coefficient of 7×10^{-13} cm³ molecule⁻¹ s⁻¹ determined by Mihele et al.[13] as necessary to simulate the measurements of the chain length of their chemical amplifier in the presence of wet air by including in the mechanism reaction 1bw. In their experiments, the observed chain length decreased at 50% rh by approximately a factor of 2 with respect to dry conditions that could not be explained only by the increase of radical wall loss. Taking into account that for the equilibrium constant they used a somewhat smaller value of $K_6 = 3 \times 10^{-19}$ cm³ molecule⁻¹, the rate constant $k_{1bw} = 6 \times 10^{-13}$ cm³ molecule⁻¹ s⁻¹ obtained in the present work well explains the observed detection sensitivity of chemical amplifiers to water vapor.

Atmospheric Implication. The assessment of the atmospheric implication of reaction 1bw needs a knowledge of k_{1bw} under various atmospheric conditions. However, Kircher and Sander[4] have found that the enhancement of the $HO_2 + HO_2$ rate constant in the presence of added water vapor does not change with pressure in the 100–700 Torr range. This allows us to assume that the effect of water on HNO₃ formation in reaction 1a also weakly depends on pressure in this range. If we apply the obtained k_{1bw} value to the conditions near the Earth's surface, we find that at 50% rh the $HO_2 + NO$ reaction appears to be a source of HNO₃ as important as the $OH + NO_2$ reaction. Also, the net loss rate of the HO_x radicals, which is dominated by the reaction of OH with NO₂, except in remote regions, will be strongly affected by the loss of HO_2 radicals in the reaction with NO. It is more difficult to predict the importance of the humidity effect at higher altitudes, where water concentration

progressively decreases, but where this decrease is partly compensated by the increase of K_6, for which a negative temperature dependence was determined by Kanno et al.[36] Further work is needed to determine water effect on reaction 1a at pressures and temperatures within the atmospheric ranges.

III. Theoretical Study

III.1. Computational Methods. The potential energy surface (PES) of the $HO_2 + NO$ reaction has been explored using a DFT approach based on the B3LYP functional and the flexible 6-311++G(d,p) basis set containing polarization and diffuse functions. This method is a good compromise between high performance and low cost for calculating accurate molecular structures, vibrational frequencies, and thermochemical properties. In his study of alkyl peroxy radicals reaction with NO, Lohr et al.[8] have shown that the DFT-UB3LYP/6-311++G(d,p) method provides reasonable thermochemistry compared to highly correlated wave functions for equilibrium structures. Analysis of electron correlation effects performed by Cremer[37] showed that DFT methods describe satisfactorily systems represented by single-determinant wave functions. Cremer has also shown that DFT methods can lead to reasonable descriptions of multireference systems (like singlet biradicals or homolytically dissociating singlet molecules) provided that broken-symmetry wave functions at unrestricted Hartree–Fock (UHF) level (mixing of HOMO and LUMO orbitals) are used. This is typically the case of the HO_2/NO system, since the PES involved in this process is of singlet multiplicity with variable numbers of open shells from zero (like HOONO and HNO₃) to two ($HO_2 + NO$, $HO + NO_2$ and biradical-like transition states). This is discussed by Zhao et al.[15] and Bach et al.[38] where UB3LYP, UQCISD, and CASSCF give energetic results in agreement with each other. This has also been recently discussed by Dibble,[39] who has shown that restricted calculations cannot account for the dissociation pathway of singlet molecules into radicals. In this work, we have used unrestricted calculations, mixing HOMO and LUMO orbitals. Minima and transition states were fully optimized and characterized by harmonic vibrational frequency analysis. Intrinsic reaction coordinate (IRC) calculations[40] have been performed to confirm the connection between the transition states with designated intermediates. When necessary, single-point energy calculations UCCSD(T)/6-311++G(d,p) have been carried out. The Gaussian03 program package[41] has been used throughout the study.

III.2. Theoretical Results and Discussion. *III.2.1. HO₂ + NO Mechanism in Absence of H₂O.* The overall calculated energy level diagram for the $HO_2 + NO$ reaction is presented in Figure 10 where the DFT-UB3LYP/6-311++G(d,p) energy values include zero-point vibrational energy corrections. The geometries corresponding to the calculated stationary points are described in Figure 11 and the energies are displayed in Table 3. Formations of $OH + NO_2$ and HNO₃ products are exothermic by 9 and 51 kcal mol⁻¹, respectively. As shown in refs 8 and 16, these DFT values agree well with the G3, QCISDT/ccPVTZ, CCSD(T)/CBS, and experimental estimates of energy values.

HOONO adduct. As already shown in previous studies, the first step of the reaction is the formation of a singlet HOONO adduct[14,15] (and references therein). Its two conformers play an important role in the overall $HO_2 + NO$ reaction since they are correlated with the products of the reaction. The most stable one corresponds to the planar *cis,cis*-HOONO stabilized by an intramolecular hydrogen bonding. The stability of this adduct with respect to the reactants is found to be 20 kcal mol⁻¹ in our DFT calculations in agreement with other B3LYP calculations (Lohr et al.,[8] 20.1 kcal mol⁻¹; Sumathi et al.,[14] 20.1 kcal
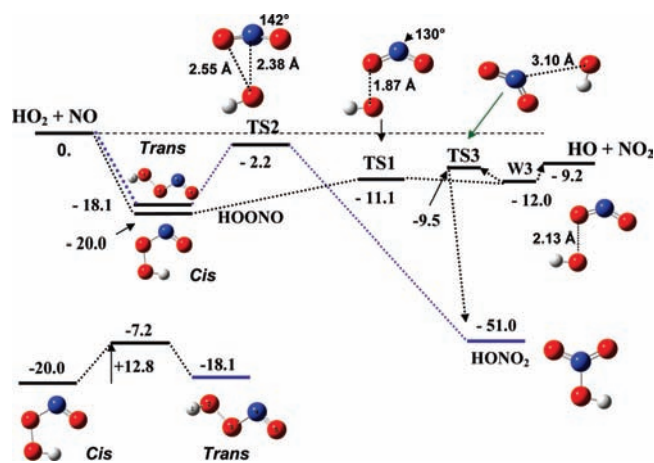
Figure 10. Schematic diagram of the potential energy surface for the $HO_2 + NO$ reaction computed at the UB3LYP/6-311++G(d,p) level. Energies including zero-point corrections in kcal mol^{-1}.

mol^{-1}; Zhang et al.,[9] 22.5 kcal.mol^{-1}) and with our single point UCCSD(T)/6-311G++(d,p) value of 21 kcal mol^{-1}. Other ab initio calculations give larger values: Lohr et al.,[8] 26.0 kcal mol^{-1} and Dixon et al.,[16] 27.3 kcal mol^{-1} at G3 and MP2/ccPVTZ levels, respectively. Another adduct is the *trans,perp*-HOONO (dihedral angles: OONO = 180°, HOON = 90°), lying 1.9 kcal mol^{-1} above the *cis,cis*-HOONO conformer. Rotational cis/trans isomerization around the O—N bond passes through a saddle point, 13 kcal mol^{-1} above *cis,cis*-HOONO. These results agree with other calculations performed at DFT and higher levels of theory like CBS-QB3 and UCCSD(T) methods (ref 15 and references therein,[42]). Several experimental groups[43−47] have detected HOONO formed in gas phase by the OH + NO_2 reaction using different spectroscopic techniques (infrared cavity ring down spectroscopy[45] and infrared action spectroscopy). The cis,cis-conformer has been derived from kinetic studies[43] to have a stability of 19.8 kcal mol^{-1} relative to the OH + NO_2 asymptote (11 kcal mol^{-1} in this work). Lester and co-workers[46] propose that the O—O bond energy is less than 16.8 kcal mol^{-1} for the *trans,perp*-HOONO. The *cis,cis*- and *trans-perp*-HOONO isomers have been characterized by examining the vibrational overtone spectrum in the region of OH bands. All the experimental determinations of the force fields of the relevant HOONO structures are in satisfying agreement with the vibrational frequencies obtained from our calculations. A third stable conformer called *cis,perp*-HOONO (OONO = 0°, HOON = 90°) lying less than 1 kcal mol^{-1} above the *cis,cis*-HOONO conformer is found in our calculations, in agreement with Li et al.[48] who have presented experimental evidence that HOONO can be observed in cis,perp-configuration in a pulsed supersonic expansion. Since this conformer is not correlated directly to any product, we shall not consider it any longer. The HOONO adducts are pure singlet species (the value of the S^2 operator is equal to 0). The HOONO adduct can undergo unimolecular pathways as described below.

HO + NO₂ Decomposition Pathway. The rupture of the (H)O—O(NO) bond is endothermic by 11 kcal mol^{-1} with respect to the *cis,cis*-HOONO adduct. We have characterized a transition state TS1 on the pathway leading to the HO + NO_2 radicals located 11 kcal mol^{-1} below the $HO_2 + NO$ reactants (and 2 kcal mol^{-1} below the OH + NO_2 products). The TS1 structure (Figure 10) is a loose transition state presenting a large elongation of the O—O bond to 1.9 Å with the five atoms in a same plane and an imaginary frequency corresponding to an elongation of the O—O bond. The electronic spin density

distribution of TS1 is typical for a biradicaloid character since the spin density is mainly on the oxygen atom of the OH group (−0.70) and is spread on the ONO group (+0.70). This result, coupled with the fact that $S^2 = 1$ shows that spin contamination is rather important. IRC calculations show that TS1 arises from the *cis,cis*-HOONO complex in agreement with the findings of Zhao et al.[15]

HNO₃ Pathway through TS2. The rearrangement of HOONO to $HONO_2$ (HNO_3) is exothermic by 31 kcal mol^{-1} and involves a transition state TS2. Our calculations show that the barrier corresponding to TS2 lies 18 kcal mol^{-1} above *cis,cis*-HOONO. This energy value is in agreement with that obtained previously at the CBS//MP2-cc-pVDZ level by Dixon et al.[16] (21.4 kcal mol^{-1}) although our geometry is tighter than theirs. Our value is much smaller than that proposed by Sumathi et al.[14] (39 kcal mol^{-1}). The reason of this discrepancy is due to the fact that they missed to perform an open-shell calculation as required for such a species (see section III.1). As a matter of fact, we reobtained the same energy value as them from a DFT-B3LYP calculation at the restricted level. The geometry of TS2 is a loose transition state where the OH group is almost parallel to the ONO plane with a O—N distance of 2.4 Å and (H)O—O bond lengths of 2.6 and 2.5 Å. In the same way as for TS1, the spin density distribution is concentrated on OH and ONO parts of TS2 (+0.90 and −0.90). IRC calculations show that TS2 arises from *trans,perp*-HOONO isomer. The fact that the DFT/UB3LYP energy of the TS2 barrier for isomerization of HOONO to HNO_3 is found slightly below the energy of the reactants (−2.2 kcal mol^{-1}) does not exclude a concerted mechanism for a minor formation of HNO_3 by isomerization reaction of the activated *trans,perp*-HOONO. A value of −3 kcal mol^{-1}, for this transition state with respect to the reagents, has also been calculated at the G2 M level by Zhu and Lin,[49] but they have not considered this pathway in the HNO_3 formation. We have also carried out single-point UCCSD(T)/6-311++G(d,p) calculations showing that TS2 is approximately at the same energy level as $HO_2 + NO$ reactants in agreement with the preceding results.

HNO₃ Pathway through W3 and TS3. IRC calculations show that TS1 is connected to a shallow well W3 (Figure 10) in which HO and NO_2 radicals are still in interaction. Once the system is above that well, it can dissociate without any barrier to OH + NO_2 radicals or isomerize toward HNO_3 through a transition state TS3, energetically located 2.5 kcal mol^{-1} above W3 (and 0.3 kcal mol^{-1} below OH + NO_2 products). TS3 is a planar loose transition state with a distance between the oxygen of the hydroxyl group and the nitrogen of the ONO part of around 3 Å. An IRC calculation shows that OH rotates around ONO to give $HONO_2$. It should be mentioned that the PES is almost flat in this region. Therefore, these stationary points are rather difficult to determine. TS3 seems to be similar to the structure 17 described in the paper of Zhao et al.[15] This is in line with the work of Chen et al.[18] in which the trajectory calculations show that, once HOONO begins to dissociate, a few trajectories undergo a rotation of OH causing the incipient fragments to return to form the stable $HONO_2$.

As a result of the exploration of this PES, it can be proposed that two paths issued from reaction 1a can lead to HNO_3 formation: one through TS2 (direct isomerization of *trans,perp*-HOONO to HNO_3) and the other one through TS1 (via W3 and TS3).

III.2.2. HO₂ + NO Mechanism in Presence of H₂O. We now examine the catalytic effect of water vapor on reaction 1a by exploring the potential energy surface and the mechanisms
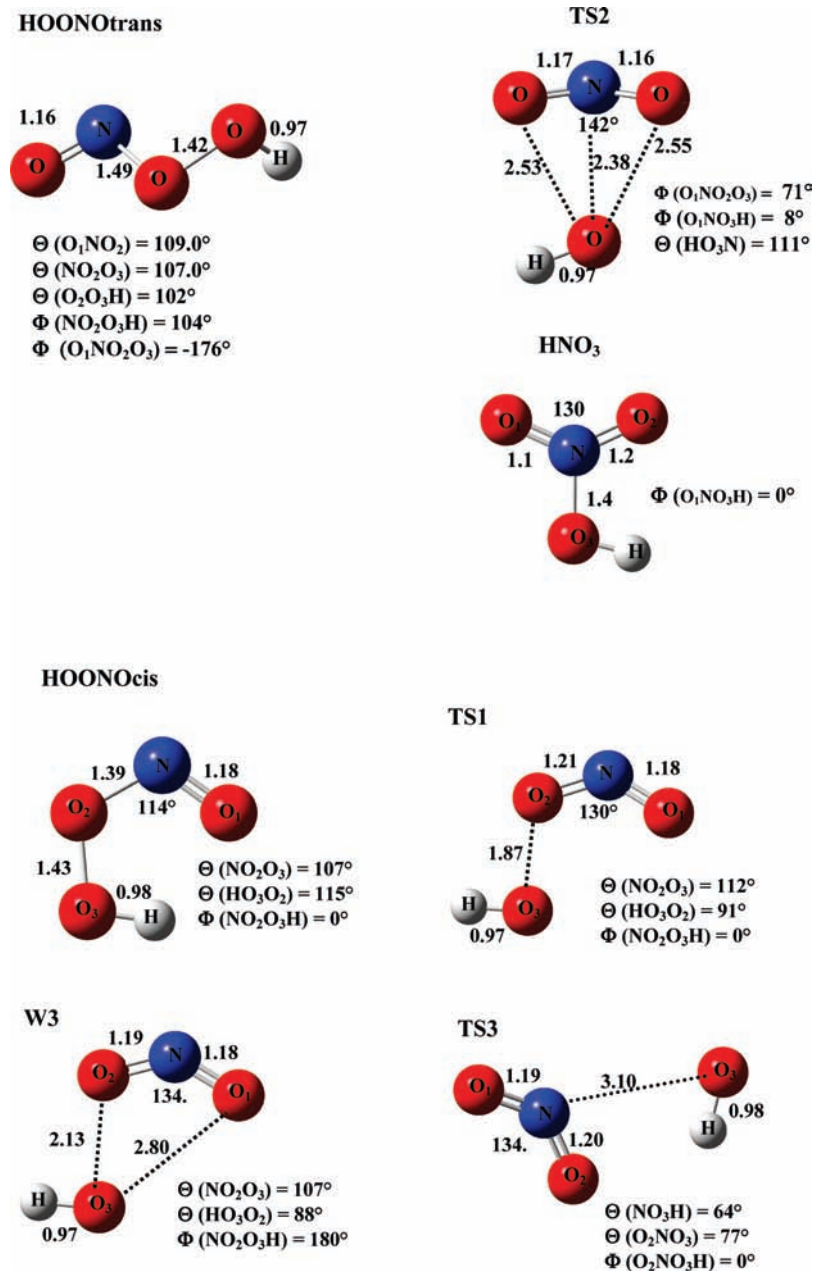
Water Vapor Effect on the HNO₃ Yield

J. Phys. Chem. A, Vol. 113, No. 42, 2009 **11337**

Figure 11. Structures of selected stationary points presented in the potential energy surface of Figure 10 for the HO₂ + NO reaction computed at the UB3LYP/6-311++G(d,p) level.

TABLE 3: Relative Electronic Energies ΔE and Zero-Point Corrected Energies ΔE_0 (kcal mol^{-1}) of the Stationary Points on the HO₂ + NO Surface at the UB3LYP/6-311++G(d,p) Level

	ΔE	ΔE_0
HO₂ + NO	0.	0.
cis,cis-HOONO	−23.0	−20.9
trans,perp-HOONO	−20.9	−18.2
TS1	−12.5	−11.1
TS2	−3.3	−2.2
W3	−13.2	−12.0
TS3	−9.4	−9.5
OH + NO₂	−8.4	−9.2
HONO₂	−55.8	−51.0

TABLE 4: Relative Electronic Energies ΔE and Zero-Point Corrected Energies ΔE_0 (kcal mol^{-1}) of the Stationary Points on the H₂O + HO₂ + NO Surface Calculated at the UB3LYP/6-311++G(d,p) Level

	ΔE	ΔE_0
H₂O + HO₂ + NO	9.8	7.2
H₂O·HO₂ + NO	0.	0.
H₂O·*cis,perp*-HOONO	−21.5	−19.6
H₂O·*trans,perp*-HOONO	−19.6	−17.6
H₂O·TS1	−8.5	−8.1
H₂O·TS2	−0.3	−0.3
H₂O·W3	−8.9	−8.8
TS3	∼7.9	∼7.8
H₂O + OH + NO₂	−1.2	−2.0
H₂O + HONO₂	−56.7	−52.4

involved by the addition of one H₂O molecule to the system. The fully optimized structures of the species involved in the reaction and the corresponding relative energy diagram (including the zero-point vibrational energy corrections) are gathered

in Table 4 and depicted in Figures 12 and 13. It is worth noticing the slight changes of the optimized geometrical parameters compared to those of the HO₂/NO system. Since H₂O exhibits
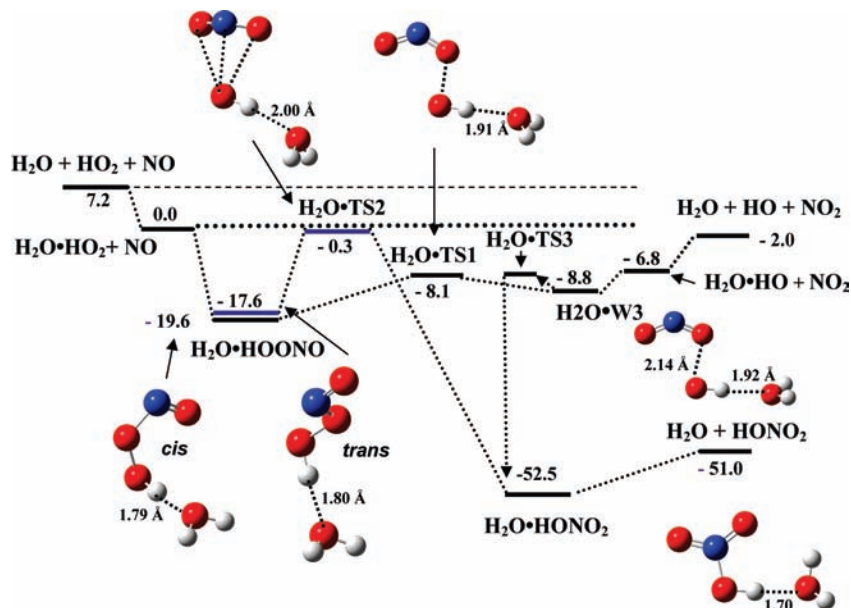
Figure 12. Schematic diagram of the potential energy surface for the $H_2O + HO_2 + NO$ reaction computed at the UB3LYP/6-311++G(d,p) level. Energies including zero-point corrections in kcal mol^{-1}.
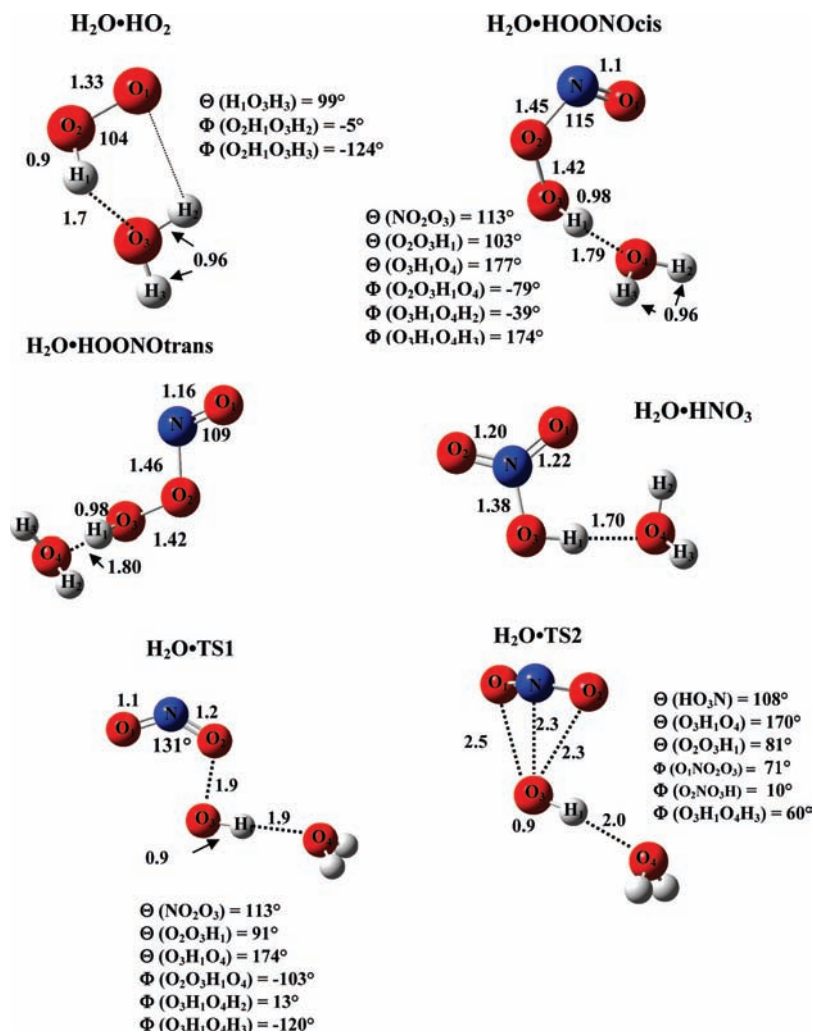
Figure 13. Structures of selected stationary points presented in the potential energy surface of Figure 12 for the $H_2O + HO_2 + NO$ reaction computed at the UB3LYP/6-311++G(d,p) level.

a very small affinity for the ONO part of the HO$_2$/NO system, the main role of the water molecule is to create a specific interaction between the oxygen atom of H$_2$O and the H atom

of HO$_2$ at an O$-$H distance between 1.8 and 2.0 Å. This H-bonding slightly perturbs the electronic structure of the different HO$_2$/NO reactants, intermediates, and transition states.

Water Vapor Effect on the HNO₃ Yield

J. Phys. Chem. A, Vol. 113, No. 42, 2009 **11339**

The energy shift associated with the formation of the $H_2O \cdot HO_2$ adduct (-7 kcal mol^{-1}) is almost the same for all these stationary points. However, due to the electronic perturbation, small energy differences from this value exist which can explain the positive effect of humidity on the formation of HNO₃.

$H_2O \cdot HO_2$ Complex. HO₂ and H₂O can form the $H_2O \cdot HO_2$ complex with a bonding energy of 7.2 kcal mol^{-1} at the UB3LYP/6-311++G(d,p) level (Figure 12), which is close to the value of 6.9 kcal mol^{-1} predicted by Aloisio and Francisco (CCSD(T)/6-311++G(2df,2p)//B3LYP/6-311++G(2df,2p) level)[34] and to the experimental value of 7.4 ± 0.7 kcal mol^{-1} from Kanno et al.[36] Structurally speaking, the hydrogen from HO₂ is weakly bound to the oxygen of the water molecule (1.77 Å). As pointed out by Aloisio and Francisco, the complex also involves an H-bonding interaction between the terminal oxygen of HO₂ and one hydrogen of H₂O (2.6 Å). A large dipole moment of H₂O (1.84 D) favors a barrierless potential energy channel for the formation of this $H_2O \cdot HO_2$ complex which is rapidly formed and thus thermalized. Then, it can react with NO to give adducts. This is strong support for choosing the $H_2O \cdot HO_2 + NO$ system as the origin of the energies.

Stable $H_2O \cdot HOONO$ Adducts. Figure 12 depicts the two main HOONO isomers in interaction with H₂O located on the PES. The more stable one, $H_2O \cdot cis$-HOONO, exhibits a geometry in which the HOONO part looks like the *cis,perp*-HOONO described in section III.2.1. The $H_2O \cdot trans$-HOONO conformer has a similar geometry as the *trans,perp*-HOONO conformer. In both conformers, the hydrogen of the OH moiety interacts with the oxygen atom of the molecule of water. $H_2O \cdot trans$-HOONO is energetically located 2 kcal mol^{-1} above the $H_2O \cdot cis$-HOONO isomer. The stabilization energy of both $H_2O \cdot cis$-HOONO and $H_2O \cdot trans$-HOONO conformers with respect to $H_2O \cdot HO_2 + NO$ level is the same as that of HOONO complexes with respect to the reactants HO₂ + NO for the HO₂/NO system.

$H_2O \cdot TS1$ and $H_2O \cdot TS2$ Transition States. The $H_2O \cdot TS1$ and $H_2O \cdot TS2$ structures have geometries similar to TS1 and TS2, with water molecules forming H-bonding with the hydroxyl fragment. IRC calculations show that $H_2O \cdot TS1$ and $H_2O \cdot TS2$ are topologically connected to $H_2O \cdot cis$-HOONO and $H_2O \cdot trans$-HOONO, respectively. The energy of $H_2O \cdot TS2$ is lowered by 7.5 kcal mol^{-1} with respect to TS2 and is now 0.3 kcal mol^{-1} below $H_2O \cdot HO_2 + NO$ reactants compared to -2.2 kcal mol^{-1} in the "no water case". We can conclude that the presence of water has a negative effect on this isomerization channel. The transition state energy of $H_2O \cdot TS1$ is only lowered by 3 kcal mol^{-1} with respect to TS1, which is less than the stabilization energy of the $H_2O \cdot HO_2$ complex but is still below the $H_2O \cdot OH + NO_2$ products. Due to these destabilization energies, the direct formation of $H_2O \cdot HONO_2$ via TS2 and the dissociation into $H_2O \cdot HO + NO_2$ are both expected to be kinetically less favorable compared to the reactions without water, the fluxes of trajectories through the transition states being smaller. In the same way, it can also be noticed that the $H_2O \cdot HO_2 + NO \rightarrow H_2O \cdot OH + NO_2$ reaction pathway is less exothermic by 2.5 kcal mol^{-1} than its equivalent without water.

$H_2O \cdot OH$, $H_2O \cdot W3$ Adducts, and $H_2O \cdot TS3$ Transition State. As in the absence of water, the transition state $H_2O \cdot TS1$ leads to a very shallow $H_2O \cdot W3$ well which can dissociate into $H_2O \cdot HO + NO_2$ and then into $H_2O + HO + NO_2$ or isomerize via a $H_2O \cdot TS3$ transition state to $H_2O \cdot HNO_3$ complex energetically located 60 kcal mol^{-1} below the reactants which can also dissociate into $H_2O + HNO_3$. As the PES is almost flat in this area, it is more difficult to localize the $H_2O \cdot TS3$ saddle point

connecting $H_2O \cdot W3$ to the $H_2O \cdot HONO_2$ complex than the TS3, and we can only state that the $H_2O \cdot TS3$ location is not higher than approximately 1 kcal/mol with respect to $H_2O \cdot W3$. As a consequence, this channel of HNO₃ formation is smoother and more open than the equivalent one in the "no-water case", which can explain the increase of HNO₃ formation in the presence of water.

In summary, from the theoretical analysis we can conclude that once the $H_2O \cdot HO_2$ complex is formed, the fluxes leading to the formation of the $H_2O \cdot HOONO$ complexes are more or less the same as those in the "no-water case". Since we know that (i) the fluxes of direct formation of HNO₃ via TS2 and dissociation to HO + NO₂ via TS1 are both slightly reduced with respect to the "no-water case" but (ii) the channel of HNO₃ formation via the $H_2O \cdot W3$ and $H_2O \cdot TS3$ structures is looking more open than in their equivalent W3 and TS3, we predict that the formation of HNO₃ will be enhanced by addition of water.

IV. Conclusions

A significant enhancement of the HNO₃ production from the HO₂ + NO reaction in the presence of water vapor was found at 298 K and 200 Torr. Assuming that this enhancement is a result of the NO reaction with $HO_2 \cdot H_2O$ hydrogen bonded complex, the obtained branching fraction of HNO₃-forming channel is found to increase from ~0.2% in reaction with HO₂ to ~7% in reaction with $HO_2 \cdot H_2O$. The theoretical quantum chemistry calculations qualitatively agree with these experimental results. Obviously, these calculations do not give any quantitative result, but the preliminary RRKM-type statistical calculations performed from elements belonging to the presented PES seem to confirm these predictions. This work will be published in a forthcoming paper. To confirm the obtained results and to clarify the mechanism of the water effect, similar experiments combined with theoretical calculations will be carried out for the fully deuterated DO₂ + D₂O system, where DNO₃ produced is expected not to interfere with the clusters formed in the ion source. Also, since the observed water effect appears to be potentially important for atmospheric modeling, the measurements of the water enhancement factor will be extended to cover as much as possible the ranges of tropospheric temperatures and pressures.

Appendix

On the Possibility of Heterogeneous Formation of Nitric Acid. As mentioned in the Introduction, the HNO₃ forming channel (1b) being very minor compared to the total reaction 1a, it is indeed important to carefully consider the possible heterogeneous processes which could interfere with channel (1b) in producing nitric acid, in both the absence and presence of water. Wall reactions are common artifacts in conventional discharge flow reactors working at low pressures of a few Torr. For example, the discharge-flow study of Sridharan et al. demonstrates interference from the first- and second-order

surface reactions.[50] Such effects are, however, strongly reduced in turbulent flow reactors, working generally at pressures higher than 100 Torr and Reynolds numbers $Re > 2000$. In our previous studies of reaction 1a[6,7] and in the present one, the flow conditions used appear to make negligible wall reactions of radicals as described below. Most of the arguments against wall contribution have been already reported in our earlier study.[7] Here we present more detailed consideration of the problem based on the properties of the turbulent flow and comparison of the results from the simple $HO_2 + NO$ and the chain $HO_2 + NO + CO + O_2$ systems.

Wall processes in a turbulent reactor are hindered due to the existence of the laminar boundary layer that reduces the wall collision frequency of the reactants. For example, Seely et al. showed that collision frequency of Cl atoms drops from 2400 s^{-1} in a laminar flow (2.5 Torr, $Re = 64$) to 60 s^{-1} in a turbulent flow (250 Torr, $Re = 4500$).[51] Theory predicts a power dependence of the thickness of a boundary layer on Re number. The well-known Schlichting formula gives $\delta = const \cdot Re^{-0.2}$.[52] In our experiments, pressure is regulated mainly by the pumping speed via a throttling valve with some correction of the nitrogen flow rate to avoid too short and too long reaction times. As Re number is determined only by the bulk mass flow of the carrier gas, it changed only from 4900 to 11000 when the pressure was varied from 70 to 600 Torr. The ratio of the respective estimated layer thicknesses is $\delta(Re = 4900)/\delta(Re = 11000) = 1.18$. The small difference between these δ values made it possible to consider the thickness as pressure-invariant. One of the consequences of the formation of the boundary layer under turbulent flow regime is that the average velocity of the gas (v_{Re}) is larger than the velocity calculated from the mass flow of the gas and the tube cross section (v). The thickness of the layer can be roughly estimated from the ratio of these velocities. The effective velocity in our TFR was determined in an earlier study using the well-determined rate constant for the $O_3 + NO$ reaction.[53] The measured $v_{Re}/v = 1.23 \pm 0.12$ ratio was found to be practically independent of Re over the 2600−10000 range. This ratio corresponds to the boundary layer thickness of $\delta = 1.17$ mm. It is worth to note that for a reactor of the same diameter, Seely et al. have estimated the boundary layer thickness as 1.5 mm at $Re = 1000$ and 0.8 mm at $Re = 10000$.[51] For the range of Re numbers used in our study, this would correspond to a change from 1 to 0.8 mm.

The possible occurrence of wall reactions can be estimated by comparing the rates of reactions in the gas phase and of mass transport of reactive species to the reactor wall. First, let us consider the *simple $HO_2 + NO$ system*, where high NO concentrations up to 1.2×10^{16} molecules cm^{-3} were used to suppress secondary reaction 4.[7] At room temperature and 200 Torr, the molecular diffusion coefficient of HO_2 in N_2 is $D = 0.75$ cm^2/s. The diffusion time through the boundary layer of $\delta = 1.17$ mm thickness is approximately $t_d \approx \delta^2/4D = 4.6 \times 10^{-3}$ s and the characteristic time for reaction with NO is $t_{HO_2+NO} = 1/(k_{HO_2+NO} [NO]) = 1/(8.8 \times 10^{-12} \cdot 1 \times 10^{16}) \cong 1 \times 10^{-5}$ s. Hence, during the time required for diffusion, the HO_2 concentration nominally reduces by a factor of 10^{-176} due to the gas phase reaction with NO. Similar estimation made for the OH radicals with the molecular diffusion coefficient of 1.2 cm^2/s, $t_d = 2.9 \times 10^{-3}$ s and $t_{OH+NO} = 1/(k_{OH+NO} [NO]) = 1/((3 \times 10^{-12})(1 \times 10^{16})) \cong 3 \times 10^{-5}$ s, gives a decreasing factor of 10^{-37}. These estimations show that in the proximity of the wall the concentration of radicals is practically zero, independently of their initial concentration in the turbulent core, and they cannot be adsorbed on the surface. In other words, the possibility

of HNO_3 formation in surface reactions of radicals (first or second order) can be ruled out because radicals simply do not reach the wall. At the same time, a constant HNO_3 signal intensity was observed by using NO concentration between 8 $\times 10^{14}$ and 1×10^{16} molecules cm^{-3}, in agreement with a gas-phase mechanism (Figure 5 in ref 7).

The absence of wall reactions in the $HO_2 + NO$ system is consistent with the fact that the same value of the branching ratio, β, was obtained in the reactor coated with halocarbon wax and in the cleaned reactor. Table 3 of ref 7 contains the results in chronological order. First experiments (lines 1−5 of Table 3) were carried out with the reactor and the injector coated with halocarbon wax. Then, the reactor was cleaned, the wax removed, and a new injector was installed. At the same time, some parts of ion optics and ion source were cleaned. Table 3 shows noticeable change of the HNO_3 to NO_2 sensitivity ratio (I_{82}/I_{46}), but the ratio of their concentrations, β, remained practically unchanged.

Our experiments also show that HNO_3 cannot be produced in a surface reaction during the initial mixing process with the estimated duration of about 0.1 ms. This mechanism can be ruled out on the basis of experiments in two reaction systems, with C_6H_{12} and CO as OH scavengers, where the radicals are regenerated along the entire length of the reaction zone and, hence, where the HNO_3 formation cannot be explained by the reactivity of radicals reaching the surface during the initial mixing process. For both chain systems the observed yield of HNO_3 is in agreement with the results obtained in the nonchain system with NO as the OH scavenger.

In the *chain $HO_2 + NO + CO$* system, used in ref 6 to study pressure and temperature dependence of β, the boundary layer does not prevent the radicals to reach the reactor wall. The chain-limiting step in our system was the $HO_2 + NO$ reaction. For the NO concentrations used ($\approx 5 \times 10^{13}$ molecules cm^{-3}), the characteristic reaction time was $t_{HO_2+NO} \cong 2.3 \times 10^{-3}$ s, which is comparable with the radical diffusion time. The radicals are regenerated on passing through the boundary layer, and their near-wall concentration is approximately the same as their concentration in the core flow. In such a situation, the gas-phase formation is indistinguishable from the second-order heterogeneous formation of a product. The measured HNO_3 yield in this system, however, is exactly the same as in the simple nonchain system, proving the absence of an exclusively heterogeneous mechanism. Besides, in the case of heterogeneous formation in such a chain system, HNO_3 yield would be independent of pressure in contrast to the observed positive linear pressure dependence.

The positive linear pressure dependence of β is generally incompatible with heterogeneous formation of HNO_3. At the same time, it is easily explained by a gas-phase mechanism, considering collisional stabilization of the formed product.[8−10,54] Regarding the observed negative temperature dependence of β, that seems to be typical for heterogeneous processes, it can be explained in terms of thermal decomposition of the intermediate HOONO complex provided TS3, the transition state for isomerization to HNO_3, lies below the $OH + NO_2$ energy.[8−10,54]

Our last argument against the surface formation of HNO_3 is based on the constancy of the branching ratio β measured in the experiments performed over a long period (7 years), under very different wall conditions. Such a reproducibility is generally not observed when wall reactions occur.

The major argument suggesting the possibility of heterogeneous formation of HNO_3 is based on the observation of significant zero-pressure intercept of the pressure dependence

Water Vapor Effect on the HNO$_3$ Yield

J. Phys. Chem. A, Vol. 113, No. 42, 2009 **11341**

of β (Figure 3 of ref 6), which contradicts to the zero intercept required by a gas-phase mechanism. The observed increase of the intercept with the decrease of temperature (Figure 6 of ref 6) could be explained, for example, by an Eley–Rideal mechanism[55] for heterogeneous reaction of adsorbed HO$_2$ with NO. At present, we have no explanation for these experimental findings.

However, such an intercept problem appears to be not specific of the HO$_2$ + NO reaction but is also common for nitrate formation in reactions of NO with alkyl peroxy radicals, RO$_2$. Similar intercepts were observed by Atkinson's group in their studies of the pressure dependence of C$_5$–C$_8$ alkyl nitrate yields,[56–58] the most recent study of Aschmann et al.[58] being undertaken in particular to verify the pressure dependence for pentyl nitrate obtained earlier.[56] Accurate measurements of the pressure dependence for both 2- and 3-pentyl nitrate yields over the 51–774 Torr range gave straight lines with significant intercepts, for which no explanations were given (corrections for the contribution from secondary gas-phase reaction did not eliminate them).[58] Unfortunately, no information is available on these intercepts as a function of temperature, as those measurements were carried out only at 297 K. It is worth also to mention, that in very recent investigations from our laboratory, apparent zero-pressure intercepts were also found in the pressure dependences of nitrate formation in the lighter C$_2$H$_5$O$_2$ + NO and iso-C$_3$H$_7$O$_2$ + NO systems.[59] The nature of these intercepts is not clear. First of all, it is necessary to note that the intercepts under discussion are the result of extrapolation to zero pressure and there is no evidence that the intercepts are true or false, i.e., an artifact of extrapolation. The explanation might be found in the complexity of the potential energy surface of the HO$_2$ + NO–HOONO–HONO$_2$ system having several potential wells. Zhang et al. suggested that the general picture of the pressure dependence for nitrate formation yield in RO$_2$ + NO reaction can display a dual falloff curve, one falloff corresponding to stabilization of the ROONO complex and another one to stabilization of the RONO$_2$ product.[9] Unfortunately, we cannot check this hypothesis, since our equipment cannot operate at pressures below 70 Torr. So, there is a need to examine low-pressure behavior of nitrates and HNO$_3$ formation in RO$_2$ + NO reactions using other techniques.

In summary, we have presented substantial arguments against important wall contribution to our measurements of the HNO$_3$ yields, β, reported in our previous papers and the present one. On the other hand, experimental facts such as the observed zero-pressure intercepts of the pressure dependences of β cannot find an explanation so far. The issue of the zero-pressure intercepts needs to be solved by further experimental investigations at low pressures (less than 50 Torr) as well as by theoretical studies.

References and Notes

(1) English, A. M.; Hansen, J. C.; Szente, J. J.; Maricq, M. M. *J. Phys. Chem. A* **2008**, *112*, 9220.

(2) Kanno, N.; Tonokura, K.; Tezaki, A.; Koshi, M. *J. Phys. Chem. A* **2005**, *109*, 3153.

(3) Stone, D.; Rowley, D. M. *Phys. Chem. Chem. Phys.* **2005**, *7*, 2156.

(4) Kircher, C. C.; Sander, S. P. *J. Phys. Chem.* **1984**, *88*, 2082.

(5) Sander, S. P.; Peterson, M.; Watson, R. T.; Patrick, R. *J. Phys. Chem.* **1982**, *86*, 1236.

(6) Butkovskaya, N. I.; Kukui, A.; Le Bras, G. *J. Phys. Chem. A* **2007**, *111*, 9047.

(7) Butkovskaya, N. I.; Kukui, A.; Pouvesle, N.; Le Bras, G. *J. Phys. Chem. A* **2005**, *109*, 6509.

(8) Lohr, L. L.; Barker, J. R.; Shroll, R. M. *J. Phys. Chem. A* **2003**, *107*, 7429.

(9) Zhang, J.; Dransfield, T.; Donahue, N. M. *J. Phys. Chem. A* **2004**, *108*, 9082.

(10) Zhang, J.; Donahue, N. M. *J. Phys. Chem. A* **2006**, *110*, 6898.

(11) Cariolle, D.; Evans, M. J.; Chipperfield, M. P.; Butkovskaya, N. I.; Kukui, A.; Le Bras, G. *Atmos. Chem. Phys.* **2008**, *8*, 4061.

(12) Cantrell, C. A.; Stedman, D. H. *Geophys. Res. Lett.* **1982**, *9*, 846.

(13) Mihele, C. M.; Mozurkewich, M.; Hastie, D. R. *Int. J. Chem. Kinet.* **1999**, *31*, 145.

(14) Sumathi, R.; Peyerimhoff, S. D. *J. Chem. Phys.* **1997**, *107*, 1872.

(15) Zhao, Y.; Houk, K. N.; Olson, L. P. *J. Phys. Chem. A* **2004**, *108*, 5864.

(16) Dixon, D. A.; Feller, D.; Zhan, C. G.; Francisco, J. S. *J. Phys. Chem. A* **2002**, *106*, 3191.

(17) Chen, C.; Shepler, B. C.; Braams, B. J.; Bowman, J. M. *J. Chem. Phys.* **2007**, *127*, 104310.

(18) Chen, C.; Shepler, B. C.; Braams, B. J.; Bowman, J. M. *Phys. Chem. Chem. Phys.* **2009**, *11*, 4722.

(19) Huey, L. G.; Hanson, D. R.; Howard, C. J. *J. Phys. Chem.* **1995**, *99*, 5001.

(20) Van Brunt, R. J.; Herron, J. T. *IEEE Trans. Electr. Insul.* **1990**, *25*, 75.

(21) Sauers, I.; Harman, G. *J. Phys. D: Appl. Phys.* **1992**, *25*, 761.

(22) Sauers, I.; Harman, G. *J. Phys. D: Appl. Phys.* **1992**, *25*, 774.

(23) Ikezoe, Y.; Matsuoka, S.; Takebe, M.; Viggiano, A. *Gas Phase Ion–Molecule Reaction Rate Constants Through 1986*; Ion Reaction Research Group of the Mass Spectroscopy Society of Japan: Tokyo, 1987 (distributed by Maruzen Co.).

(24) Huey, L. G. *Mass Spectrom. Rev.* **2007**, *26*, 166.

(25) Arnold, S. T.; Viggiano, A. A. *J. Phys. Chem. A* **2001**, *105*, 3527.

(26) Slusher, D. L.; Pitteri, S. J.; Haman, B. J.; Tanner, D. J.; Huey, L. G. *Geophys. Res. Lett.* **2001**, *28*, 3876.

(27) Huey, L. G.; Lovejoy, E. R. *Int. J. Mass Spectrom. Ion Processes* **1996**, *155*, 133.

(28) Elrod, M. J.; Ranschaert, D. L.; Schneider, N. J. *Int. J. Chem. Kinet.* **2001**, *33*, 363.

(29) Davidson, J. A.; Fehsenfeld, F. C.; Howard, C. J. *Int. J. Chem. Kinet.* **1977**, *9*, 17.

(30) Finlayson-Pitts, B. J.; Wingen, L. M.; Summer, A. L.; Syomin, D.; Ramazan, K. A. *Phys. Chem. Chem. Phys.* **2003**, *5*, 223.

(31) Ramazan, K. A.; Wingen, L. M.; Miller, Y.; Chaban, G. M.; Gerber, R. B.; Xantheas, S. S.; Finlayson-Pitts, B. J. *J. Phys. Chem. A* **2006**, *110*, 6886.

(32) Nelander, B. *J. Phys. Chem. A* **1997**, *101*, 9092.

(33) Aloisio, S.; Francisco, J. S.; Friedl, R. R. *J. Phys. Chem. A* **2000**, *104*, 6597.

(34) Aloisio, S.; Francisco, J. S. *J. Phys. Chem. A* **1998**, *102*, 1899.

(35) Bohn, B.; Zetzsch, C. *J. Phys. Chem. A* **1997**, *101*, 1488.

(36) Kanno, N.; Tonokura, K.; Koshi, M. *J. Geophys. Res.* **2006**, *111*, D20312.

(37) Cremer, D. *Mol. Phys.* **2001**, *99*, 1899.

(38) Bach, R. D.; Dmitrenko, O.; Estévez, C. M. *J. Am. Chem. Soc.* **2003**, *125*, 16204.

(39) Dibble, T. S. *Atmos. Environ.* **2008**, *42*, 5837.

(40) Gonzalez, C.; Schlegel, H. B. *J. Phys. Chem.* **1989**, *90*, 2154.

(41) *Gaussian 03, Revision C.02*, Frisch, M. J.; Trucks, G. W.; Schlegel, H. B.; Scuseria, G. E.; Robb, M. A.; Cheeseman, J. R.; Montgomery, J. A., Jr.; Vreven, T.; Kudin, K. N.; Burant, J. C.; Millam, J. M.; Iyengar, S. S.; Tomasi, J.; Barone, V.; Mennucci, B.; Cossi, M.; Scalmani, G.; Rega, N.; Petersson, G. A.; Nakatsuji, H.; Hada, M.; Ehara, M.; Toyota, K.; Fukuda, R.; Hasegawa, J.; Ishida, M.; Nakajima, T.; Honda, Y.; Kitao, O.; Nakai, H.; Klene, M.; Li, X.; Knox, J. E.; Hratchian, H. P.; Cross, J. B.; Bakken, V.; Adamo, C.; Jaramillo, J.; Gomperts, R.; Stratmann, R. E.; Yazyev, O.; Austin, A. J.; Cammi, R.; Pomelli, C.; Ochterski, J. W.; Ayala, P. Y.; Morokuma, K.; Voth, G. A.; Salvador, P.; Dannenberg, J. J.; Zakrzewski, V. G.; Dapprich, S.; Daniels, A. D.; Strain, M. C.; Farkas, O.; Malick, D. K.; Rabuck, A. D.; Raghavachari, K.; Foresman, J. B.; Ortiz, J. V.; Cui, Q.; Baboul, A. G.; Clifford, S.; Cioslowski, J.; Stefanov, B. B.; Liu, G.; Liashenko, A.; Piskorz, P.; Komaromi, I.; Martin, R. L.; Fox, D. J.; Keith, T.; Al-Laham, M. A.; Peng, C. Y.; Nanayakkara, A.; Challacombe, M.; Gill, P. M. W.; Johnson, B.; Chen, W.; Wong, M. W.; Gonzalez, C.; Pople, J. A. *Gaussian 03, Revision C.02*; Gaussian, Inc.: Wallingford, CT, 2004.

(42) McGrath, M. P.; Rowland, F. S. *J. Chem. Phys.* **2005**, *122*, 134312.

(43) Hippler, H.; Nasterlak, S.; Striebel, F. *Phys. Chem. Chem. Phys.* **2002**, *4*, 2959.

(44) Nizkorodov, S. A.; Wennberg, P. O. *J. Phys. Chem. A* **2002**, *106*, 855.

(45) Bean, B. D.; Mollner, A. K.; Nizkorodov, S. A.; Nair, G.; Okumura, M.; Sander, S. P.; Peterson, K. A.; Francisco, J. S. *J. Phys. Chem. A* **2003**, *107*, 6974.

(46) Pollak, I. B.; Konen, I. M.; Li, E. X. J.; Lester, M. I. *J. Chem. Phys.* **2003**, *119*, 9981.

(47) Fry, J. L.; Nizkorodov, S. A.; Okumura, M.; Roehl, C. M.; Francisco, J. S.; Wennberg, P. O. *J. Chem. Phys.* **2004**, *121*, 1433.

(48) Li, E. X. J.; Konen, I. M.; Lester, M. I.; McCoy, A. B. *J. Phys. Chem. A* **2006**, *110*, 5607.

(49) Zhu, R. S.; Lin, M. C. *J. Chem. Phys.* **2003**, *107*, 10667.

(50) Sridharan, U. C.; Reimann, B.; Kaufman, F. *J. Chem. Phys.* **1980**, *73*, 1286.

(51) Seely, J. V.; Jayne, J. T.; Molina, M. J. *Int. J. Chem. Kinet.* **1993**, *25*, 571.

(52) Schlichting, H *Boundary Layer Theory*: McGraw-Hill: New York, 1979.

(53) Kukui, A.; Borissenko, D.; Laverdet, G.; Le Bras, G. *J. Phys. Chem. A* **2003**, *107*, 5732.

(54) Barker, J. R.; Lohr, L. L.; Shroll, R. M.; Reading, S. *J. Phys. Chem. A* **2003**, *107*, 7434.

(55) Steinfeld, J. I.; Francisco, J. S.; Hase, W. L. *Chemical Kinetics and Dynamics*; Prentice-Hall: Englewood Cliffs, NJ, 1998.

(56) Atkinson, R.; Carter, W. P. L.; Winer, A. M. *J. Phys. Chem.* **1983**, *87*, 2012.

(57) Atkinson, R.; Aschmann, S. M.; Winer, A. M. *J. Atmos. Chem.* **1987**, *5*, 91.

(58) Aschmann, S. M.; Long, W. D.; Atkinson, R. *J. Phys. Chem.* **2006**, *110*, 6617.

(59) Butkovskaya, N.; Kukui, A.; Le Bras, G. To be published.